ISSN 1818-2712
J Nucl Med Tech
核 醫 技 學 誌

Journal of Nuclear Medicine Technology 核醫技術學雜誌

核醫技術學雜誌

Journal of Nuclear Medicine Technology

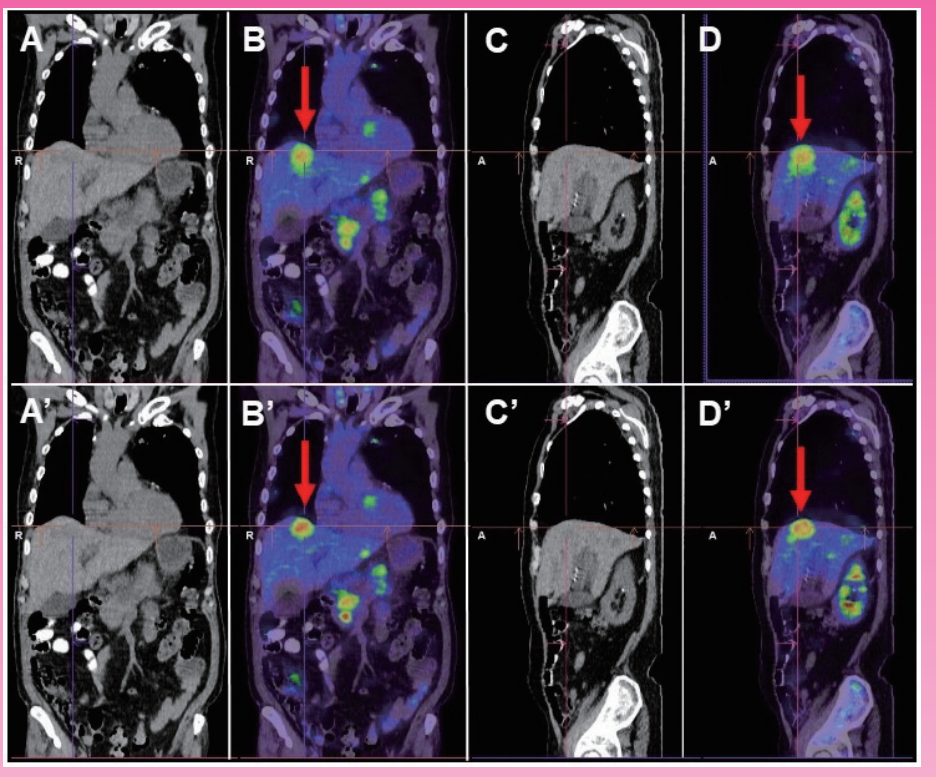

The red long thick arrow indicates a focal area with heterogeneous increased FDG uptake in the liver S8. (A, A': coronal CT; B, B': coronal PET/CT fusion; C, C': sagittal CT; D, D': sagittal PET/CT fusion). Respiration-gated images (OncoFreeze AI with data-driven respiration gating; A', B', C' and D') and ungated images (static; A, B, C, D) were reconstructed. The liver S8 lesion measured maxSUV 7.6, meanSUV 5.1 and metabolic tumor volume 19.1 cm^3 in ungated images (static; A, B, C, D). The liver S8 lesion measured maxSUV 8.7, meanSUV 6.1 and metabolic tumor volume 13 cm^3 in respiration-gated images (OncoFreeze AI with data-driven respiration gating; A', B', C' and D'). The liver S8 lesion measured in CT image (2.6x2.3 cm), ungated images (2.6x2.9 cm) and respiration-gated images (2.6x2.5 cm).

Volume 22 Number 1 December 2025

第二十二卷 第一期 中華民國一一四年十二月

Published by NM Technology Committee, the Society of Nuclear Medicine, R.O.C.

中 華 民 國 核 醫 學 學 會

醫 技 委 員 會 發行

Volume 22 Number 1 Pages 1-58 December 2025

核醫技術學雜誌
Journal of Nuclear Medicine Technology

發行人 (Publisher)
吳彥雯 (Yen-Wen Wu)
亞東紀念醫院

創刊人 (Original Publisher)
黃延城 (Yan-Cherng Huang)
臺北榮民總醫院

總編輯 (Editor-in-Chief)
王秀珊 (Hsiu-Shan Wang)
三軍總醫院

副總編輯 (Associate Editorsin-Chief)
陳怡勳 (Yi-Hsun Chen)
嘉義基督教醫院
鄭雯文 (Wen-Wen Cheng)
淡水馬偕紀念醫院
林雯君 (Wen-Chun Lin)
高雄榮民總醫院

執行秘書 (Production Secretary)
張婉柔 (Wan-Jo Chang)
台大癌醫中心分院

編輯委員 (Editorial Board)
北區
陳恩賜 (En-Shih Cheng)
三軍總醫院
王安美 (An-Mei Wang)
台北馬偕醫院
黃奕琿 (Yih-Hwen Huang)
臺大醫院
蔡佳玲 (Chia-Lin Tsai)
長庚醫院
辜啓泰 (Chi-Tai Ku)
新光醫院
梁瑋玲 (Wei-Ling Liang)
和信醫院
黃馨美 (Hsing-Mei Huang)
國泰醫院
陳雅凰 (Ya-Huang Chen)
亞東醫院
黃雅婕 (Ya-Chieh Huang)
萬芳醫院

中區
周國堂 (Kuo-Tang Chou)
臺中榮民總醫院
顏國揚 (Kuo-Yang Yen)
中國醫學大學附設醫院
張白容 (Pai-Jung Chang)
中山醫學大學附設醫院
姜繼宗 (Chi-Tsung Chiang)
中國醫學大學附設醫院
黃政凱 (Cheng-Kai Huang)
中港澄清醫院
張添信 (Tien-Hsin Chang)
台中慈濟醫院
詹況栗 (Kuang-Li Chang)
國軍臺中總醫院

南區
陳宜伶 (Yi-Ling Chen)
高雄醫學院附設醫院
李世昌 (Shih-Chang Li)
成大醫院
王文祥 (Wen-Hsiang Wang)
義大醫院
俞長青 (Chang-Ching Yu)
高雄榮民總醫院
鄭時維 (Shih-Wei Cheng)
屏東基督教醫院
莊欣慧 (Hsin-Hui Chuang)
國軍左營醫院
許幼青 (Yu-Ching Hsu)
大林慈濟醫院
張紫綺 (Tzu-Chi Chang)
柳營奇美醫院

東區
陳惠萍 (Hui-Ping Chen)
台東基督教醫院

核醫技術學雜誌

第 22 卷第 1 期　中華民國核醫學學會醫技委員會學誌　中華民國 114 年 12 月發行

原　著

病例報告

Journal of Nuclear Medicine Technology

The Official Publication of NM Technology Committee, the Society of Nuclear Medicine, R.O.C.

ISSN 1818-2712

Volume 22, Number 1 December 2025

Original Articles

Case Reports

中華民國 93 年 11 月 20 日創刊

發　　行：中華民國核醫學學會 秘書處

理 事 長：吳彥雯

醫技委員會主任委員：陳惠萍

總 編 輯：王秀珊

雜誌編輯總顧問：杜高瑩

投稿信箱：susanwang@ndmctsgh.edu.tw

會　　址：220 新北市板橋區南亞南路二段 21 號 核子醫學科轉核醫學學會

電　　話：02-7731-5328

電子信箱：tsnm.tw@snm.org.tw

劃撥帳號：19781819

戶　　名：中華民國核醫學學會

印　　刷：宇晨企業有限公司 yuchen68@ms51.hinet.net

地　　址：台北市和平東路二段 151 號 6 樓

電　　話：02-2703-7667　傳真：02-2703-3381

不同掃描模式對骨質密度測量精準度之影響：以兩種腰椎假體爲例

羅浚哲[1]　張砡慈[1]　黃琪雯[1,2]

[1] 中山醫學大學附設醫院 核子醫學科
[2] 中山醫學大學 醫學研究所

摘要

前言：準確測量腰椎骨密度 (BMD) 對於診斷骨質疏鬆症至關重要，這是一種因人口老齡化而日益嚴重的全球健康問題。雙能量 X 射線吸收測定儀 (DXA) 被視爲測量 BMD 的黃金標準。本研究比較三種 DXA 掃描模式 (Array、Fast Array 和 Turbo) 對兩種不同密度腰椎假體中的 BMD 測量準確性。

材料與方法：本研究使用兩種假體：模擬健康骨骼的假體 A(1.230 g/cm^2) 和模擬骨質疏鬆骨骼的假體 B(0.940 g/cm^2)。使用 DXA 設備對每種掃描模式和假體進行 10 次掃描。分析的指標包括骨礦含量 (BMC)、掃描面積 (AREA) 和 BMD，並通過盒形圖和單因子方差分析 (ANOVA) 評估數據變異性與差異性。

結果：在三種掃描模式下，兩種不同假體的平均 BMD 結果 (g/cm^2) 存在統計顯著差異 ($p < 0.05$)。雖然所有模式的平均 BMD 與參考值均有顯著差異 ($p < 0.05$)，但 Turbo 模式的偏差最大。相較之下，Array 和 Fast Array 模式之間的平均 BMD 差異最小，顯示其測量結果更爲一致。

結論：Fast Array 模式在精準度與效率之間達到平衡，是腰椎 BMD 評估的理想選擇。Array 模式雖然精準度較高，但掃描時間較長；Turbo 模式速度更快，但穩定性較差。臨床上應根據需求選擇合適模式，以確保 BMD 測量結果的可靠性。

關鍵詞：雙能量 X 射線吸收測定儀、骨質密度、腰椎假體

核醫技學誌 2025;22:1-5

接受日期：2025 年 1 月 13 日
通訊作者：羅浚哲
聯絡地址：台中市南區建國北路一段 110 號
聯絡電話：04-24739595 ext. 32002
電子郵件：cshc173@csh.org.tw

前言

腰椎骨質密度 (BMD) 的準確測量對於評估骨骼健康和診斷骨質疏鬆症具有重要意義。骨質疏鬆症是一種常見的代謝性骨病，隨著全球人口老化的增長，骨質疏鬆症已成爲全球主要關注的健康問題 (1)。由於骨折的短期 (例如住院、手術) 和長期後果 (例如殘疾、失能)，骨質疏鬆症對人群的經濟負擔也在持續增加 (2)。準確的 BMD 測量有助於疾病的早期干預和有效治療。骨質疏鬆症是一種全球性的公共健康問題，隨著人口老齡化，其發生率呈現持續上升的趨勢，因此，準確的骨密度評估對於疾病的早期診斷和治療至關重要。雙能量 X 射線吸收儀 (Dual-energy X-ray Absorptiometry, DXA) 作爲目前臨床上最常用的骨密度測量工具，因其非侵入性、快速性和高精準性受到廣泛應用。然而，在 DXA 掃描中，掃描時間和精準度之間的平衡始終是研究的焦點。針對不同的臨床需求，本研究使用 DXA 掃描機的三種模式 (Array、Fast Array 和 Turbo)，以探討其性能差異。本研究旨在評估兩種不同腰椎假體在三種掃描模式下的骨質密度精準度，並透過分析其骨礦含量 (BMC)、掃描區域 (AREA) 及骨質密度 (BMD) 的表現，探討最佳的掃描模式選擇，望爲臨床實踐提供依據。

材料與方法

研究材料

本研究使用兩種不同腰椎假體作爲主要實驗材料，這兩種假體在形狀、大小及材質上存在一定差異，能夠模擬兩種類型的腰椎結構及骨骼密度特徵。假體 A (Lunar Expert phantom) 模擬健康骨骼狀態，具有較高的骨密度 1.230 g/cm^2，而假體 B(Hologic DXA Phantom) 模擬骨質疏鬆的病理狀態，骨密度相對較低 0.940 g/cm^2。

本次使用的骨質密度掃描機 (Discovery Wi DEXA, Hologic, Inc.) 是本研究的核心設備，其高靈敏度和可靠性使其成爲研究骨密度的標準工具。圖一與圖二展示了

三種掃描模式 (Array、Fast Array 和 Turbo) 的影像差異，涵蓋從高精準度到高效率的需求範圍。每種掃描模式進行 10 次重複掃描，確保數據具有統計意義。

分析方法

分析的主要指標包括 BMC、AREA 和 BMD，這些指標是評估骨質密度精準度的主要參數。其中，BMC 反映骨骼中的礦物質總量，AREA 測量掃描的骨骼區域面積，而 BMD 是 BMC 與 AREA 的比值，更是評估骨骼強度的關鍵指標。我們同時利用盒形圖比較 BMD 在三種模式數據上的變異性，進一步探討不同掃描模式對數據的穩定性影響。統計分析採用適當的檢定方法 ANOVA 分析，判斷數據間的顯著性差異 ($p < 0.05$)。

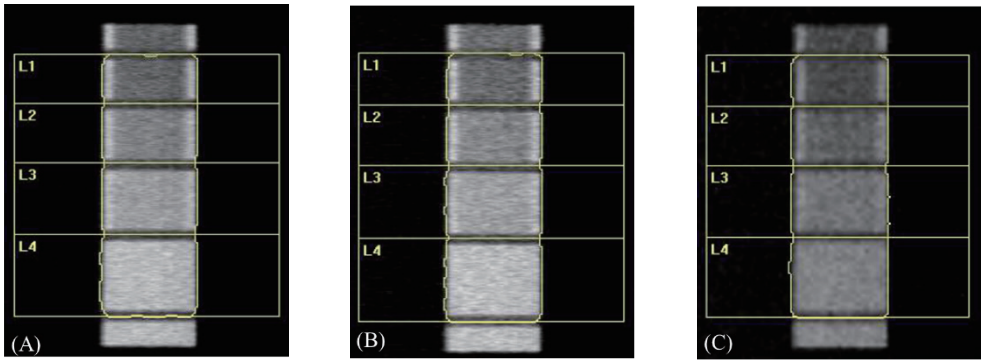

圖 1. 假體 A (Lunar Expert phantom) 在不同掃描模式下影像 (A) Array 模式、(B) Fast Array 模式、(C) Turbo 模式

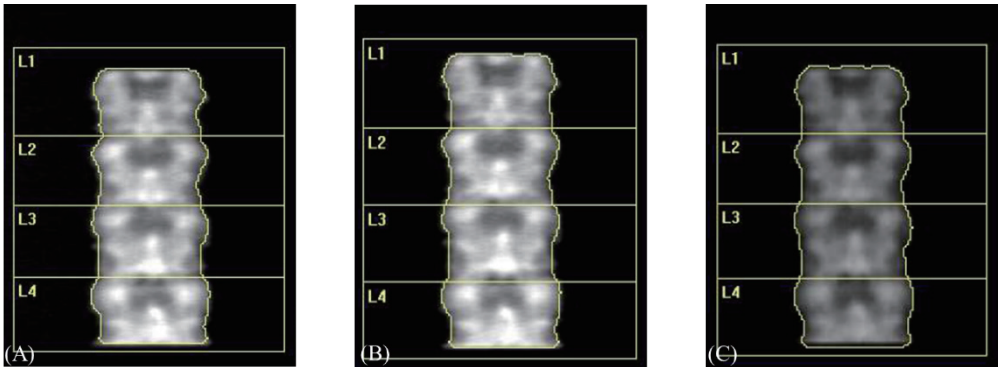

圖 2. 假體 B (Hologic DXA Phantom) 在不同掃描模式下影像 (A) Array 模式、(B) Fast Array 模式、(C) Turbo 模式

結果與討論

表一、表二呈現了兩種不同特性假體在三種掃描模式的平均 BMD 結果 (g/cm²) 以及掃描時間；不同掃描模式下的 BMD 測量結果均呈現統計上的顯著差異 ($p < 0.05$)。表三提供了三種掃描模式的平均 BMD 結果與參考值 (1 g/cm²) 之間的差異比較。圖三、圖四顯示儘管 BMD 結果與參考值之間存在顯著差異 ($p < 0.05$)，但與 Array 和 Fast Array 模式相比，Turbo 掃描模式的差異更大。與此發現一致的是，與其他兩對掃描模式之間的差異相比，Array 和 Fast Array 之間的平均 BMD 差異皆是最小的。

DXA 已在世界各地用於診斷骨質疏鬆症以及作爲骨折風險預測的組成部分，特別是在停經後女性。不同廠牌 DXA 具有不同的空間解析度、掃描時間和輻射劑量，根據對患者人體測量特徵的主觀評估提供不同的掃描模式。先前的假體研究主要聚焦於單一假體的研究，本篇研究使用兩種不同標定密度的腰椎假體進行三種不同掃描模式差異的研究。兩種不同假體的測量結果顯示，不同材質、密度和結構的假體可能對數據穩定性產生一定影響，進一步研究這些差異對掃描模式選擇的重要性將是未來的研究方向。

表一　假體 A (Lunar Expert phantom) 在不同模式下掃描結果

	AREA	BMC	BMD	Scan time(s)
	Mean ±SD	Mean ±SD	Mean ±SD	Mean
Array	55.09±0.24	55.07±0.22	1.00±0.00	78
Fast Array	55.31±0.27	55.13±0.20	1.00±0.00	46
Turbo	53.34±2.12	51.64±1.71	0.97±0.01	23
p-value	<0.05	<0.05	<0.05	N/A

表二　假體 B (Hologic DXA Phantom) 在不同模式下掃描結果

	AREA	BMC	BMD	Scan time(s)
	Mean±SD	Mean ±SD	Mean ±SD	Mean
Array	55.35±0.24	53.10±0.57	0.96±0.00	92
Fast Array	55.13±0.23	52.43±0.25	0.95±0.00	79
Turbo	52.57±0.19	48.03±0.20	0.91±0.01	39
p-value	<0.05	<0.05	<0.05	N/A

表三　兩種假體在不同掃描模式下 ΔBMD 結果

	假體 A	假體 B
	ΔBMD*	
	Mean ±SD	Mean ±SD
Array	0.02±0.00	-0.23±0.00
Fast Array	0.01±0.00	-0.23±0.00
Turbo	-0.03±0.01	-0.26±0.00
p-value	<0.05	<0.05

*ΔBMD= 在不同模式下掃描 BMD 結果 - BMD 參考值

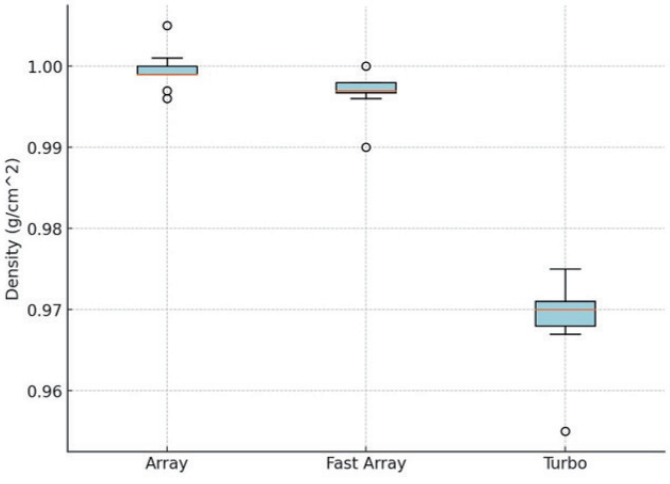

圖 3.　假體 A (Lunar Expert phantom) 在不同掃描模式下 BMD 散佈情形

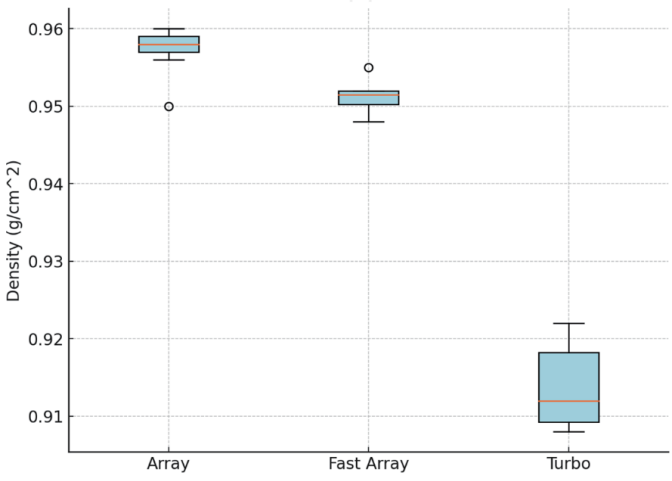

圖 4.　假體 B (Hologic DXA Phantom) 在不同掃描模式下 BMD 散佈情形

本研究的限制包括使用假體模型而非人類受試者進行比較，儘管如此，研究設計仍能有效模擬兩種不同 BMD 狀態下的測量情境；第二個限制是我們在研究中沒有比較 T 和 Z 分數的差異，因爲我們使用了假體模型，所以我們認爲直接專注 BMD 測量結果，並非參考年齡的 T 和 Z 分數。因此，我們必須承認本研究結果更適用於 BMD 長期監測，這已在先前研究發表過 (3)。第三個限制是我們在研究中沒有比較輻射劑量。然而，Bandirali 等人先前對此進行了研究 (4,5)。

結論

從本研究結果可知 Fast Array 模式在精準度與效率之間達到平衡，是腰椎 BMD 評估的理想掃描模式。Array 模式雖然精準度較高，但掃描時間較長；Turbo 模式速度更快，但穩定性較差。臨床上使用應根據需求選擇合適掃描模式，以確保 BMD 測量結果的可靠性。本研究建議，根據臨床需求和時間條件選擇最適合的掃描模式，以確保骨密度測量結果的可靠性，從而爲臨床決策提供更強有力的支持。

參考文獻

1. Alejandro P, Constantinescu F. A review of osteoporosis in the older adult: an update. Rheum Dis Clin North Am. 2018;44:437-51.
2. Si L, Winzenberg TM, Jiang Q, et al. Projection of osteoporosis-related fractures and costs in China: 2010-2050. Osteoporos Int. 2015;26:1929-37.
3. Staal KP, Roos JC, Manoliu RA, et al. Variations in diagnostic performances of dual-energy X-ray absorptiometry in the northwest of The Netherlands. Osteoporos Int. 2004;15:335-44.
4. Bandirali M, Sconfienza LM, Aliprandi A, et al. In vivo differences among scan modes in bone mineral density measurement at dual-energy X-ray absorptiometry. Radiol Med. 2014;119:257-60.
5. Bandirali M, Poloni A, Sconfienza LM, et al. Short-term precision assessment of trabecular bone score and bone mineral density using dual-energy X-ray absorptiometry with different scan modes: an in vivo study. Eur Radiol. 2015;25:2194-8.

The Effect of Different Scanning Modes on the Accuracy of Bone Mineral Density Measurements: A Study Using Two Lumbar Spine Phantoms

Chun-Che Lo[1], Yu-Tzu Chang[1], Chi-Wen Huang[1,2]

[1]*Department of Nuclear Medicine, Chung Shan Medical University Hospital, Taichung, Taiwan*
[2]*Institute of Medicine, Chung Shan Medical University*

Abstract

Introduction: Accurate lumbar spine BMD measurement is vital for diagnosing osteoporosis, a global health concern exacerbated by population aging. Dual-energy X-ray Absorptiometry (DXA) is the gold standard for its precision. This study compares BMD accuracy across three DXA modes—Array, Fast Array, and Turbo—using two lumbar spine phantoms with varying densities.

Materials and Methods: Two phantoms were used, one phantom A (1.230 g/cm²) simulating healthy bone, and phantom B (0.940 g/cm²) mimicking osteoporotic bone. A Hologic DXA device performed 10 scans per mode per phantom. Metrics analyzed included BMC, AREA, and BMD. Variability and differences were assessed using box plots and ANOVA.

Results: Significant differences ($p < 0.05$) in BMD were found across modes for both phantoms. Turbo mode showed greater deviations from reference values, while Array and Fast Array modes were more consistent.

Conclusion: Fast Array mode balances precision and efficiency, making it ideal for spinal BMD assessment. Array mode provides higher accuracy but requires longer scanning times. Turbo mode is Faster but less reliable. Mode selection should align with clinical needs to ensure reliable BMD results.

Keywords: Dual-energy X-ray Absorptiometry (DXA), Bone Mineral Density (BMD), Lumbar Spine Phantoms

J Nucl Med Tech 2025;22:1-5

Received 2025/1/13
Corresponding author: Chun-Che Lo
Address: No. 110, Section 1, Jianguo N. Rd., Taichung City 402, Taiwan, R.O.C.
Tel: 04-24739595 ext. 32002; E-mail: cshc173@csh.org.tw

注射針具對醫護人員體外輻射劑量的影響

王寶英[1]　郭彥伶[1]　蔡承延[1]　王瑾妍[1]　吳宜臻[1]

[1] 義大醫療財團法人義大醫院核子醫學科

摘要

核子醫學使用放射性同位素製劑經注射，口服或吸入給予受檢者在其體內分佈吸收，依據組織器官生理或病理的變化，達到功能性的檢查目的，然而對於施打放射性同位素製劑人員而言，如何在給藥的過程中降低體外輻射曝露是一項重要的課題。本研究探討使用不同注射針具對給藥者體外輻射暴露之差異。利用輻射偵檢儀 (surver meter) 進行注射放射性同位素製劑時體外暴露量測，以鉛針套包覆針筒之下推注活度 20mCi 之 $^{99m}TcO4^-$ 時，計測距射源 30 公分處之輻射暴露劑量。分別以注射針頭直接注射，去針頭後接 3-way 再接頭皮針及生理食鹽水注射，記錄：(a-1) 汲取 20 mCi 之 $^{99m}TcO4^-$ 後，使用含鉛針套且未取下針頭的注射前之暴露劑量。(a-2) 取下針頭後之注射前暴露劑量。(b) 將針管內 $^{99m}TcO4^-$ 完全推出注射期間之最大暴露劑量。(c) 推完 $^{99m}TcO4^-$ 後含鉛針套之注射後暴露劑量。比較各種不同方式間暴露劑量之差異。結果顯示暴露劑量 (a-1) 以針頭直接注射前之暴露劑量爲 32.59 (±6.86) μSv / hr，(a-2) 取下針頭後注射前之暴露劑量爲 21.46 (±5.86) μSv / hr，(b) 注射期間之針頭與頭皮針最大暴露劑量分別爲 75.78 (±20.73)μSv / hr、 149.35 (±17.0) μSv / hr，(c) 注射後針頭與頭皮針暴露劑量分別爲 14.47 (±3.54) μSv / hr、126.19 (±24.98) μSv / hr，以生理食鹽水回沖後暴露劑量爲 42.60 (±24.7) μSv / hr。以注射針頭直接注射方式可達到最低的體外輻射暴露。因此，建議工作人員於注射放射性同位素製劑時，採用此方式以降減輻射暴露。

關鍵詞：體外曝露、放射性同位素製劑、頭皮針

核醫技學誌 2025;22:7-10

接受日期：2025 年 5 月 20 日
通訊作者：王瑾妍
聯絡地址：高雄市燕巢區角宿里義大路 1 號 義大醫院 核子醫學科
聯絡電話：07-6150011-2313
電子郵件：102210ed@gmail.com

前言

「醫療曝露品質保證作業」有效確保受檢者於放射醫療相關檢查時所接受的輻射曝露爲合理且準確。核子醫學放射性同位素製劑體內攝影檢查不同於放射診斷攝影是以體外儀器(X 光機，CT) 輸出放射線做爲取像方式，可透過電壓、電流與曝光時間的調控及良好的屏蔽設計，有效確保受檢者的實際輻射曝露劑量，並降低工作人員體外暴露。而核子醫學使用放射性同位素製劑經由注射，口服或吸入方式給予病人以進行生理性檢查，輻射暴露來自非密封性放射性同位素製劑，除了廣爲人知的「時間、距離、屏蔽」三大防護原則外，如何有效降低工作人員執行常規作業時之體外輻射暴露，尤其是新進人員訓練期間，不熟練的操作加長了接觸放射性同位素的時間進而使體外輻射暴露增加。雖然自動注射系統的使用，已被證實能有效減少輻射劑量，提升工作安全性 [1-3]，但並未普遍應用於傳統核醫檢查。在現有的工作條件下，工作人員如何在給藥的過程中降低體外輻射曝露？本實驗探討放射性同位素製劑因使用不同注射針具而導致工作人員所接受之體外暴露差異，希望藉由不同的注射方式達到降低工作人員體外輻射暴露，進而達到合理抑低 (ALARA，As Low As Reasonably Achievable) 之目標。

材料與方法

核子醫學體內攝影檢查以骨骼掃描 (Bone scan) 爲大宗，故實驗採用骨骼掃描所使用的放射性同位素 Tc-99m 及成人劑量 20mCi，且因注射體積影響注射時間與單位活度，單位活度亦會干擾實驗過程中暴露劑量的測量 [4]，參考一般骨骼掃描 ^{99m}Tc-MDP 製劑爲 1~1.2 c.c.，實驗中控制輻射源爲 $^{99m}TcO4^-$ 活度 20mCi 體積爲 1.2 c.c.。本研究使用測量儀器爲輻射偵檢儀 (surver meter)(廠牌：SE/ 型號：Inspector)，注射針具爲 2.5c.c. Terumo 附針塑膠針筒及 25 號頭皮針，實際進行注射時工作人員與注射位置 (手部) 的距離大約 20~30 公分 (圖一)，實驗數據以距離射源 30 公分處進行測量。本實驗著重於注射針

具在注射時對體外暴露的影響，故實驗中需排除因放射性藥物推注到病人體內所造成的輻射劑量干擾，模擬推進病人體內的 $^{99m}TcO4^-$ 以鉛屏蔽之，以確保所偵測的數值爲注射過程中單純因不同針具或注射方式所產生之差異。

圖 1. 注射時工作人員與注射位置 (手部) 的距離

以 2.5 c.c. 注射針筒汲取 20 mCi 之 $^{99m}TcO4^-$ 1.2 c.c.，記錄距離 30 公分處 (a-1) 含鉛針套注射前之暴露劑量 (n=40)，(a-2) 取下針頭並接上 3-way 再接頭皮針及生理食鹽水後含鉛針套注射前之暴露劑量 (n=20，直接推注法則略)，(b) 將針管內 $^{99m}TcO4^-$ 完全推出 (模擬臨床將放射性同位素製劑推注至受檢者體內) 注射期間之最大暴露劑量 (針頭，n=20/ 頭皮針，n=20)，(c) 推完 $^{99m}TcO4^-$ 後含鉛針套之注射後暴露劑量 (針頭，n=20/ 頭皮針，n=20)。(d) 接 3-way 及頭皮針者於推完 $^{99m}TcO4^-$ 後以生理食鹽水回沖一次之注射後暴露劑量 (n=20)，比較各種不同注射方式與條件間之差異。

結果

經過輻射偵檢儀測量距離射源 30 公分處的體外暴露劑量，(a-1) 直接注射針頭含鉛針套注射前之暴露劑量爲 32.59 (±6.86) μSv/hr (n=40)，(a-2) 取下針頭換接 3-way 及頭皮針注射前暴露劑量爲 21.46(±5.86) μSv/hr (n=20，直接推注法針頭不取下)，(b) 推注 $^{99m}TcO4^-$ 至鉛屏蔽的注射期間最大暴露劑量爲：直接注射針頭 75.78 (±20.73) μSv/hr (n=20)，頭皮針 (包含外接 3-way 及生理食鹽水) 149.35 (±17.0) μSv/hr (n=20)，(c) 推完 $^{99m}TcO4^-$ 後含鉛針套之注射後暴露劑量爲：直接注射針頭 14.47 (±3.54) μSv/hr，頭皮針 126.19 (±24.98) μSv/hr，(d) 頭皮針外接 3-way 及生理食鹽水於 $^{99m}TcO4^-$ 推注完後以生理食鹽水回沖一次針管之注射後暴露劑量爲：42.6 (±24.7) μSv/hr (表一)。

表一 不同注射條件體外暴露值

	注射前暴露劑量 (μSv/hr)	注射期間暴露劑量 (μSv/hr)	注射後暴露劑量 (μSv/hr)	注射後回沖洗生理食鹽水暴露劑量 (μSv/hr)
直接注射針頭 (Mean ± SD)	32.59 ± 6.86	75.78 ± 20.73	14.47 ± 3.54	—
頭皮針 (Mean ± SD)	21.46 ± 5.86	149.35 ± 17.00	126.19 ± 24.98	42.60 ± 24.7

討論

在實驗結果中，直接注射針頭含鉛針套之暴露劑量主要來自未被鉛針套屏蔽的針頭部分 (圖二)，當將針頭取下換上 3-way 及頭皮針時體外暴露可由 32.59 (±6.86) μSv/hr 降至 21.46 (±5.86) μSv/hr 降幅達 34.15%，但在推注過程中頭皮針軟管無鉛屏蔽造成推注過程最大暴露劑量急劇增加至原本的 1.97 倍，使用針頭直接注射，不僅執行時間較短，且最大暴露劑量亦較頭皮針低 49.26% (75.78(±20.73) / 149.35(±17.0)μSv/hr)，注射結束後含鉛針套之輻射暴露依舊是以針頭直接注射最低，沖洗生理食鹽水後頭皮針次之，單純外接頭皮針的暴露量最高，爲直接注射針頭的 8.7 倍。

除了體外輻暴露劑量明顯的差異外，操作過程中，將針頭取下換上頭皮針的動作，或 $^{99m}TcO4^-$ 推注完後以生理食鹽水回沖針管，都增加了工作人員直接接觸輻射的時間，有違輻射防護時間縮短原則。當然，實際幫病人注射時，更長的處理時間所增加的輻射暴露還必需加上已注入病人身上無屏蔽的輻射。較長的接觸時間搭配較高的輻射暴露，進一步凸顯了傳統針頭相較於頭皮針的優劣。

結論

由本研究結果可獲知，於注射放射性同位素製劑時，以針頭直接注射方式最佳。但於臨床作業時尚需考量檢查守則之規範，例如心血流第一次穿流灌注 (first-pass) 對檢查使用之示蹤劑要求須爲 0.3 ~ 0.5 c.c [5]，過大的注射體積將會影響其分析結果，且需借助 3-way 及頭皮針以利後續生理食鹽水將 $^{99m}TcO4^-$ 儘速推入心室。亦需考量受檢者生理狀態選擇適當的注射器具，當然，在合理抑低的原則下直接採用針筒所附加之針頭爲受檢者注射，不但可以減少頭皮針軟管處無鉛屏蔽使工作人員所接受額外輻射曝露亦可減少注射後輻射廢棄物的數量。因此，是否卸下針頭改接頭皮針，應依受檢者狀況及檢查需求，選擇最適當的注射方式。

本研究未探討不同放射性同位素 (如 I-131, Ga-67, Tl-201…等) 或放射性同位素鍵結不同載體 (如 MDP, MAA, DTPA.. 等) 後是否有相同之結果。

圖 2.　未被鉛針套屏蔽的針頭部分

References

1. Townsend DW, Bendriem B. Technologist radiation exposure and patient safety improved with automated FDG dosage preparation and injection system. J Nucl Med. 2014;55(Suppl 1):2655.
2. Bergeron G, Makris N, Smart C. Delivery methods of radiopharmaceuticals: exploring global strategies to minimize occupational radiation exposure. J Nucl Med Technol. Published online November 12, 2024. doi:10.2967/jnmt.124.268043
3. Romer T, Riklund K, Johansson L, et al. Occupational radiation dosimetry assessment using an automated infusion device for positron-emitting radiotracers. Radiat Prot Dosimetry. 2013;155(3):309–314. doi:10.1093/rpd/ncs199
4. 王寶英，吳宜臻。 探討外部作爲對放射碘全身影像之影響及應對措施，中華民國核醫學學會 2022 年會暨國際學術研討會
5. Milena J. Henzlova, MD, Manuel D. Cerqueira, MD, Christopher L. Hansen, MD, Raymond Taillefer, MD, and Siu-Sun Yao, MD. ASNC IMAGING GUIDELINES FOR NUCLEAR CARDIOLOGY PROCEDURES . American Society of Nuclear Cardiology. 2009

Effects of Different Injection Needle Devices on External Radiation Exposure to Medical Personnel

Pao-Yin Wang[1], Yan-Ling Guo[1], Cheng-Yen Tsai[1], Jin-Yan Wang[1], Yi-Chen Wu[1]

[1]*Department of Nuclear Medicine, E-DA Hospital, Kaohsiung, Taiwan*

Abstract

In nuclear medicine, radiopharmaceuticals are administered via injection, oral ingestion, or inhalation to allow their distribution and absorption within the body, facilitating functional imaging based on physiological or pathological changes in tissues and organs. However, for medical personnel administering these radiopharmaceuticals, minimizing external radiation exposure during the injection process is a key concern. This study investigates the impact of different injection devices on external radiation exposure to the operator. Using a survey meter, radiation exposure was measured during the injection of 20 mCi of $^{99m}TcO4^-$ while the syringe was shielded with a lead cover. Exposure doses were measured at a distance of 30 cm from the source under the following conditions: (a-1) before injection with the lead-shielded syringe and needle attached, (a-2) after removing the needle but before injection, (b) maximum exposure during the injection process with direct needle and scalp vein sets, and (c) after completing the injection with the lead-shielded syringe. In addition, exposure was measured following a saline flush. The results showed that the pre-injection exposure dose with the needle attached (a-1) was 32.59 (±6.86) μSv/hr, and 21.46 (±5.86) μSv/hr after removing the needle (a-2). During injection (b), maximum exposure for direct needle injection and scalp vein sets were 75.78 (±20.73) μSv/hr and 149.35 (±17.0) μSv/hr, respectively. Post-injection exposure (c) for needle and scalp vein sets were 14.47 (±3.54) μSv/hr and 126.19 (±24.98) μSv/hr, respectively, while the saline flush resulted in 42.60 (±24.7) μSv/hr. Among all methods, direct needle injection yielded the lowest external radiation exposure. Therefore, to reduce radiation exposure during radiopharmaceutical administration, direct injection using a standard needle is recommended.

Keywords: External exposure, Radiopharmaceuticals, Scalp vein set

J Nucl Med Tech 2025;22:7-10

Received 2025/5/20
Corresponding author: Jin-Yan Wang
Address: No.1, Yida Road, Jiaosu Village, Yanchao District, Kaohsiung City 82445, Taiwan, R.O.C.
Tel: 07-6150011-2313; E-mail: 102210ed@gmail.com

Evaluation of Counting Consistency of two Arduino Geiger-Müller Counter Kits Under Varying Radiation Intensities

Fa-Shun Tsai, Tai-Lin Jiang, Lin-Chun Ou, Wan-Ting Yin, Po-Hsun Chen, Cheng-Hui Lee

Division of PET Center, Shin Kong Wu Ho-Su Memorial Hospital, Taipei, Taiwan

Abstract

Introduction: Geiger counters are radiation detectors used for detecting ionizing radiation. Due to their simple structure, low cost, and ease of use, Geiger counters are widely utilized in nuclear physics, medicine, and industry. This study utilized two Geiger-Müller counter kits to perform count statistics and half-life assessments, analyzing the consistency of counting performance between the kits.

Materials and Methods: The experiment utilized Arduino Geiger-Müller counter kits (CAJOE, Model: GC-1602-NANO) with J305βγ Geiger tubes. Each Geiger-Müller counter kit was designated as Kit A and Kit B, then linked to a computer via a USB connection. The Tera Term terminal monitoring software was used to record the count values transmitted by the Arduino Nano circuit board.

Background count test: Counts per minute, or CPM, were recorded for 60 seconds per session in an environment devoid of a radioactive source, and this process was repeated 240 times. Counting statistics test: Each kit was positioned 1 cm away from a radioactive ^{137}Cs with an activity of 114.2 μCi, and counts were recorded continuously for 120 mins. Half-life test: A radioactive source of ^{18}F-FDG with an activity of 6 μCi was fixed 1 cm away from the Geiger-Müller counter, and counts were recorded for 180 mins. The decay curve was fitted to estimate the half-life.

Results: The background count rate for Kit A averaged 19.33 ± 4.16 CPM, while Kit B exhibited a slightly lower background rate of 15.69 ± 3.82 CPM. When exposed to a ^{137}Cs source, Kit A recorded an average activity of 68777.88 ± 190.39 CPM, whereas Kit B demonstrated significantly higher activity at 64898.40 ± 271.90 CPM.In the half-life determination experiment, the recorded decay curves for both kits followed an exponential trend. The data for Kit A were best fitted by the equation: $y=11935e^{-0.006095x}$ corresponding to a calculated half-life of 113.71 minutes. For Kit B, the fitted decay function was: $y=9919.9e^{-0.006179x}$ yielding a half-life of 112.17 minutes. Both values are in close agreement with the theoretical physical half-life of ^{18}F-FDG, which is 109 minutes, thereby validating the reliability and precision of the decay measurements obtained using both kits.

Conclusion: The experimental results confirm that the Geiger-Müller counter kits can effectively detect basic ionizing radiation and can be applied in radiology and radiation protection education. However, due to performance discrepancies between the kits, count values may vary under the same radiation intensity.

Keywords: Geiger-Müller counter, Geiger tube, Counting statistics, Half-life, Ionizing radiation

J Nucl Med Tech 2025;22:11-20

Received 2025/6/19
Corresponding author: Fa-Shun Tsai
Division of PET Center, Shin Kong Wu Ho-Su Memorial Hospital, Taipei, Taiwan
Address: No. 95, Wenchang Rd., Shilin Dist., Taipei City 111, Taiwan (R.O.C.)
Division of PET Center
E-mail: T005629@ms.skh.org.tw

Introduction

Medical professionals are among the workers most frequently exposed to radiation because they may do X-ray imaging or other technical tasks that expose them to ionizing radiation, sometimes known as radiation[1]. Ionizing radiation, encompassing nuclear radiation, consists of electromagnetic waves or subatomic particles with sufficient energy to ionize matter by displacing electrons from atoms or molecules. This process can lead to molecular instability and chemical reactions, which are fundamental in various applications, including medical imaging, radiation therapy, and nuclear physics. Given its potential to alter atomic structures, ionizing radiation plays a critical role in scientific and industrial fields, yet its interaction with biological tissues necessitates rigorous safety protocols[2, 3].

Ionizing radiation does not produce immediate sensory cues that are perceptible to the human senses of vision, hearing, or touch. This necessitates the use of specialized instruments for its detection and quantification. One of the most frequently used devices for this purpose is the Geiger counter, a radiation detection instrument that functions by measuring electrical pulses generated when ionizing radiation interacts with a gas-filled tube. The invention of the first prototypes of counters which would later be called Geiger counters, or Geiger-Müller counters, actually dates back to 1908, when the German physicist Hans Wilhelm Geiger, working together with Rutherford, developed a system capable of detecting the passage of single alpha particles. Geiger counters are of paramount importance in a variety of contexts, including environmental monitoring, the inspection of nuclear facilities, the implementation of radiation protection protocols and scientific research[4, 5]. These instruments provide real-time readings of radiation intensity, thus making them indispensable in many of the aforementioned applications.

Since its inception, the Geiger counter has been widely utilized not only as a professional instrument for fundamental and applied research but also in educational and amateur fields, serving as a basic tool for science enthusiasts to explore the world of radiation[6]. In recent years, advancements in low-cost microelectronics have made the manufacturing and commercialization of fully-equipped DIY Geiger counters feasible, even at remarkably affordable prices. The proliferation of low-cost devices has further expanded the possibilities of conducting experiments and activities in various aspects of daily life[7]. At present, numerous websites, blogs, and personal pages offer DIY Geiger counter projects or related commercial kits. Microcontroller boards with serial ports, such as Arduino, enable the transmission of pulse signals from DIY Geiger counters to computers or the storage of data via memory cards, thereby facilitating more convenient data processing[5, 8-13].

Manufacturers of commercially produced Geiger counters provide quality control and calibration test reports to verify the performance of their devices, which is a feature lacking in DIY Geiger counters. Theoretically, counters of the same model should yield similar counting values, though statistical fluctuations and detection efficiency may result in slight variations. To assess whether low-cost DIY Geiger counters exhibit unacceptable individual discrepancies, this study conducted count statistics and half-life counting tests using two Geiger-Müller counter kits. The objective was to evaluate the consistency of counting performance across different conditions for both counter kits.

Materials and Methods

In this study, the Geiger-Müller counter kit (CAJOE, Model: GC-1602-NANO) and the J305βγ Geiger tube were utilized. These two counter kits were designated as Kit A and Kit B, as illustrated in Figure 1. Kit A was equipped with a J305βγ tube manufactured in 2021, while Kit B featured a tube produced in 2022. The experimental code was developed and uploaded using the Arduino IDE. The user interface of the Arduino IDE and the fundamental code utilized in this study are depicted in Figure 2. The program code was configured to transmit cumulative counts every 60 seconds, followed by a reset to zero, thereby recording the counts per minute (CPM). The Arduino Nano circuit board was connected to a computer via a USB cable, and the Tera

Term port monitoring software was employed to log the counts received from the Arduino Nano board.

To ensure the stability of experimental data, the operating voltage was adjusted to 400 volts prior to each experiment in accordance with the manufacturer's recommendations. Furthermore, data collection commenced only after the kits had been powered on for three minutes, allowing the counters to reach a stable operational state.

Background Count Measurement: Two Geiger-Müller counter kits were placed in close proximity and operated for four hours to determine the baseline count value. Counting Statistics Test: This experiment employed cesium-137 (Isotope Product Laboratories, Model: CA818-843-7000) as the standard radioactive source, with an activity of 114.26 μCi on the day of measurement. Cesium-137 has a half-life of 30.05 years, which is substantially longer than the experimental period, therefore its activity can be considered constant throughout the experiment. The Geiger-Müller counter was positioned 1 cm from the cesium-137 source, and the count value was recorded 120 times, each for a duration of 60 seconds. ^{18}F Half-Life Test: A 6 μCi sample of ^{18}F-FDG was placed 1 cm from the Geiger-Müller counter, and the count value was recorded 180 times at 60 second intervals. The half-life was determined using a curve-fitting equation.

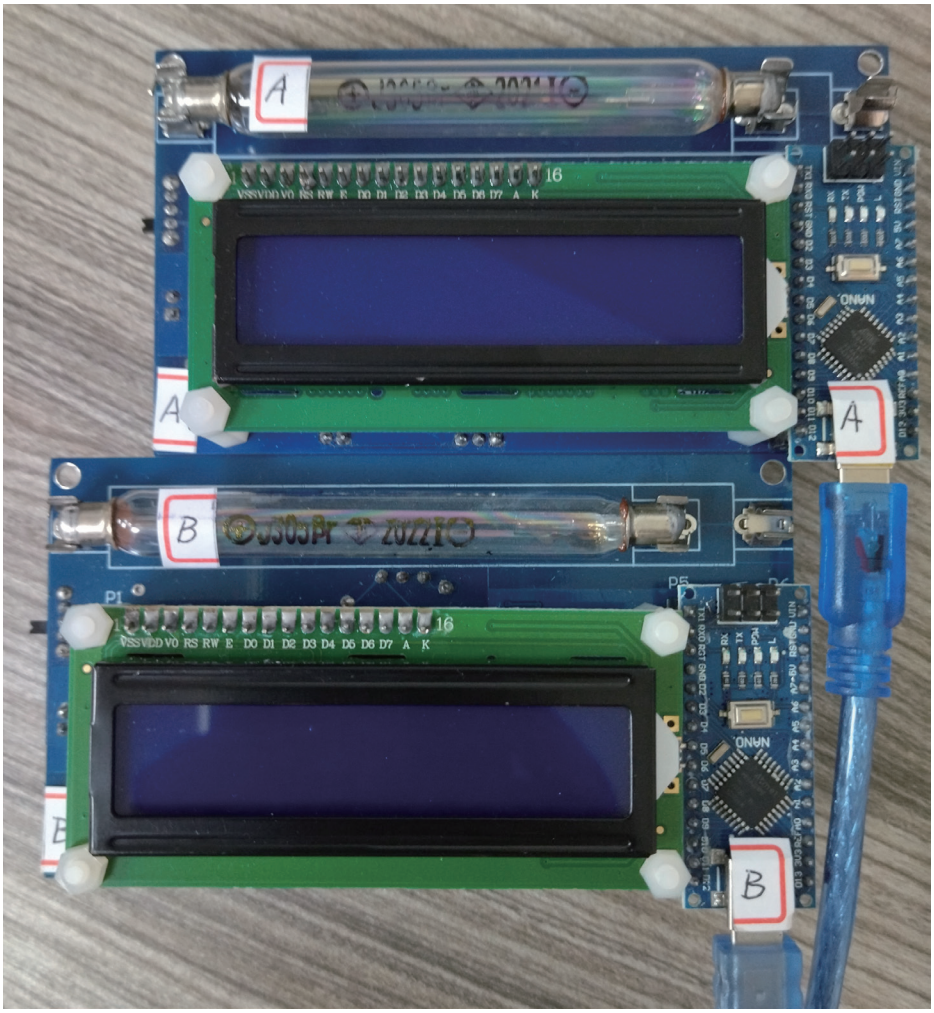

Figure 1. The Geiger-Müller counter kit (CAJOE, Model: GC-1602-NANO) is equipped with a J305βγ Geiger tube and an Arduino nano circuit board. These two counter kits were designated as Kit A and Kit B.

Figure 2. The user interface of the Arduino IDE and the basic code of this experiment. The program code was configured to transmit cumulative counts every 60 seconds.

Result

As shown in Figure 3, the background count rate measurements for Kit A and Kit B yielded average values of 19.33 ± 4.16 counts per minute (CPM) and 15.69 ± 3.82 CPM, respectively. The results of the ^{137}Cs radioactive source test are presented in Figure 4, with Kit A recording an average count rate of Kit A recorded an average activity of 68777.88 ± 190.39 CPM, while Kit B recorded a slightly lower average of 64898.40 ± 271.90 CPM. In the ^{18}F half-life test, as shown in Figure 5, the measured count rate curves exhibited a clear exponential decay pattern over time. The fitted decay curve for Kit A was described by the equation $y=11935e^{-0.006095x}$ from which the calculated half-life was 113.71 minutes, based on the standard exponential decay formula. Similarly, the fitted curve for Kit B was $y=9919.9e^{-0.006179x}$ yielding a calculated half-life of 112.17 minutes. The half-life values derived from both kits closely approximate the known physical half-life of ^{18}F-FDG, which is 109 minutes, thereby confirming the accuracy and consistency of the measurements. After changing the Y-axis in Figure 5 to a logarithmic scale, the experimental results of Kit A and Kit B appear as two parallel straight lines, as shown in Figure 6. In order to determine the correlation between the two sets of counters, we plot the count rate values of the two sets of counters over time. The correlation plot between the count rates measured by Kit A and Kit B is shown in Figure7. The solid line shows the result of a linear fit, with a slope equal to 0.839.

Discussion

The Geiger-Müller counter is a gas-filled radiation detection device that consists of a tube filled with gas connected to a high-voltage circuit. It operates by utilizing the ionization of gas caused by radiation to detect the presence of radioactive particles. A typical GM tube consists of a chamber filled with a mixture of gases and contains two electrodes, between which there is a potential difference of several hundred volts. The cathode is a conductive wire positioned along the central axis of the chamber, while the anode is a metal tube with its inner surface coated with a conductive material or wrapped with a helical wire. The Geiger tube model employed in this work is J305βγ, a tin oxide cathode with a coaxial cylindrical thin shell shape that is used in pulsed halogen tubes. When radiation strikes the tube's window, it interacts with the inert gas inside, leading to ionization. This process frees electrons from atoms, which

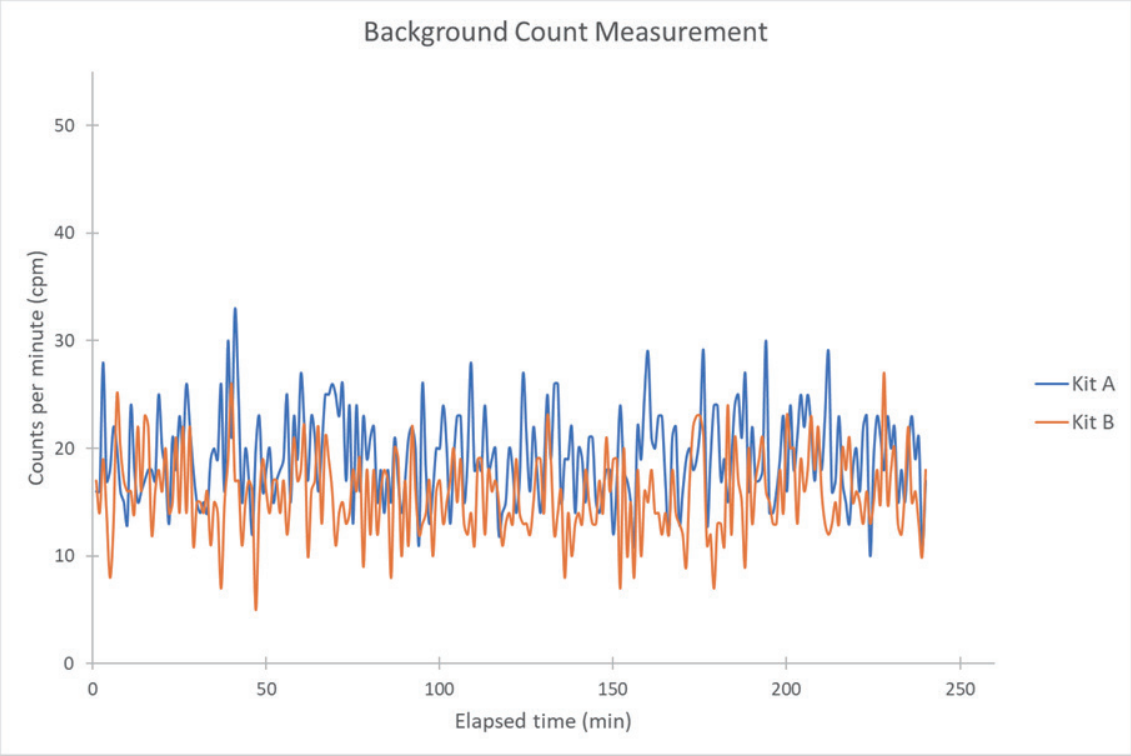

Figure 3. Elapsed Time vs. CPM in the Background counting test.

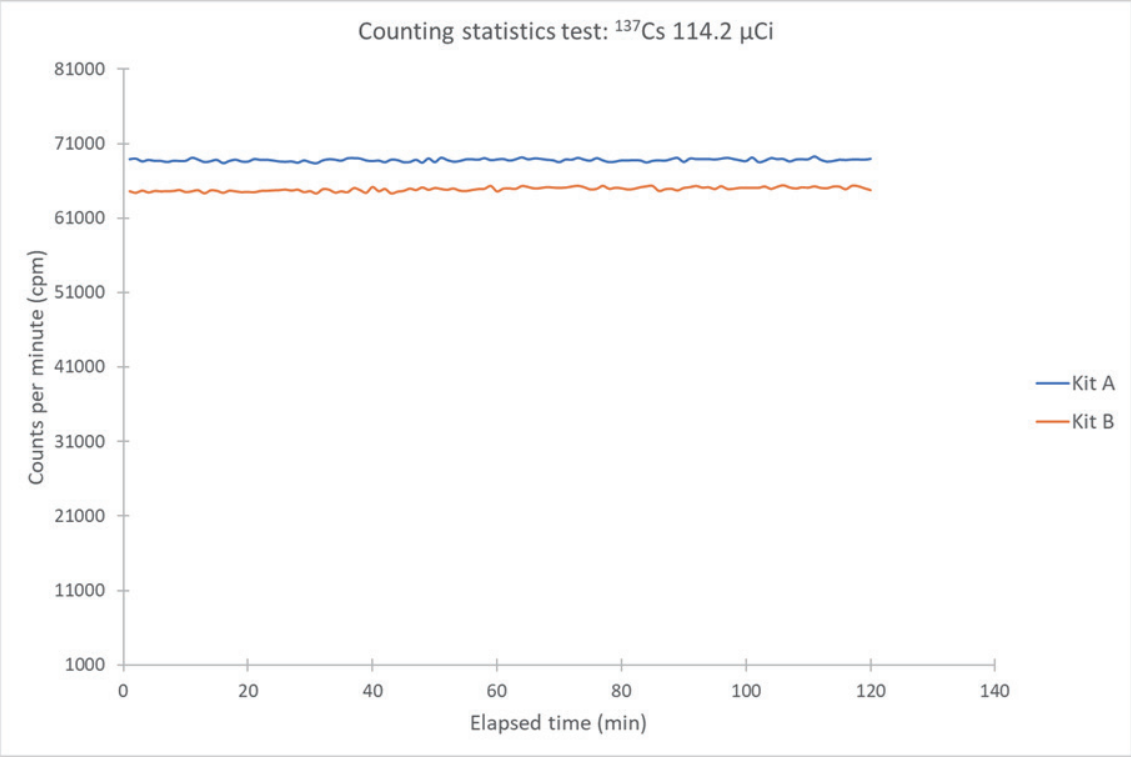

Figure 4. Elapsed Time vs. CPM in the ^{137}Cs counting test.

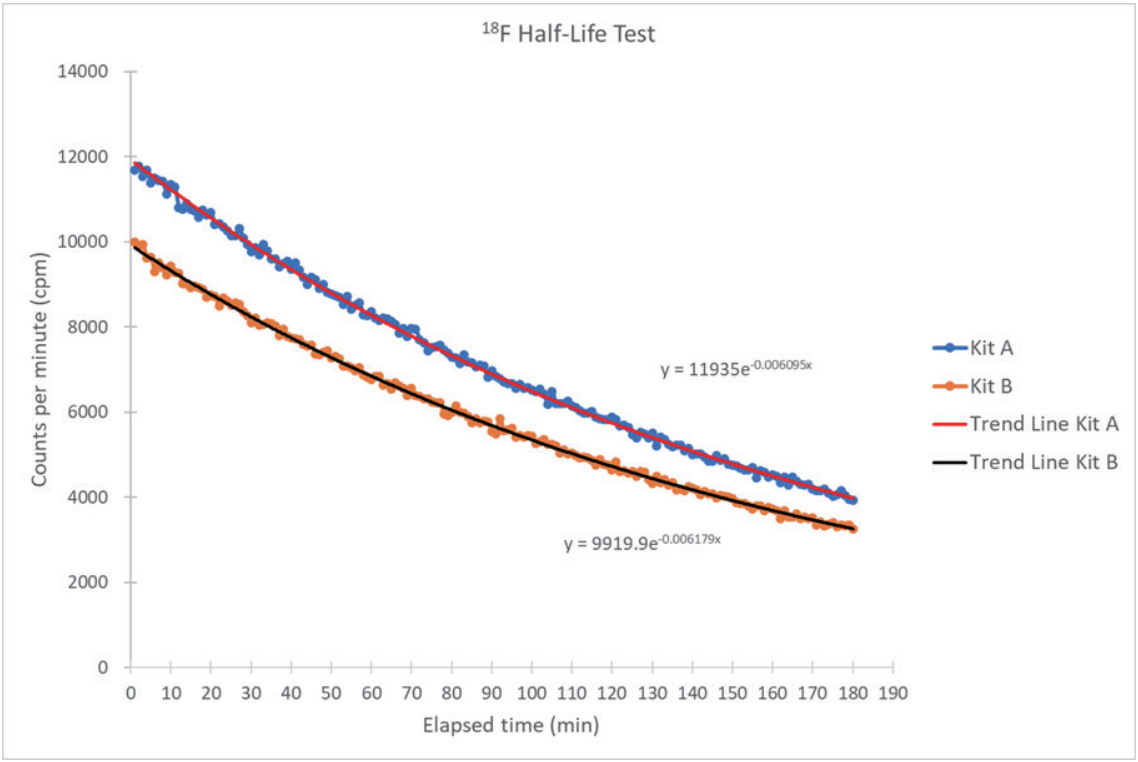

Figure 5. ^{18}F-FDG half-life counting curve and exponential decay curve fitting

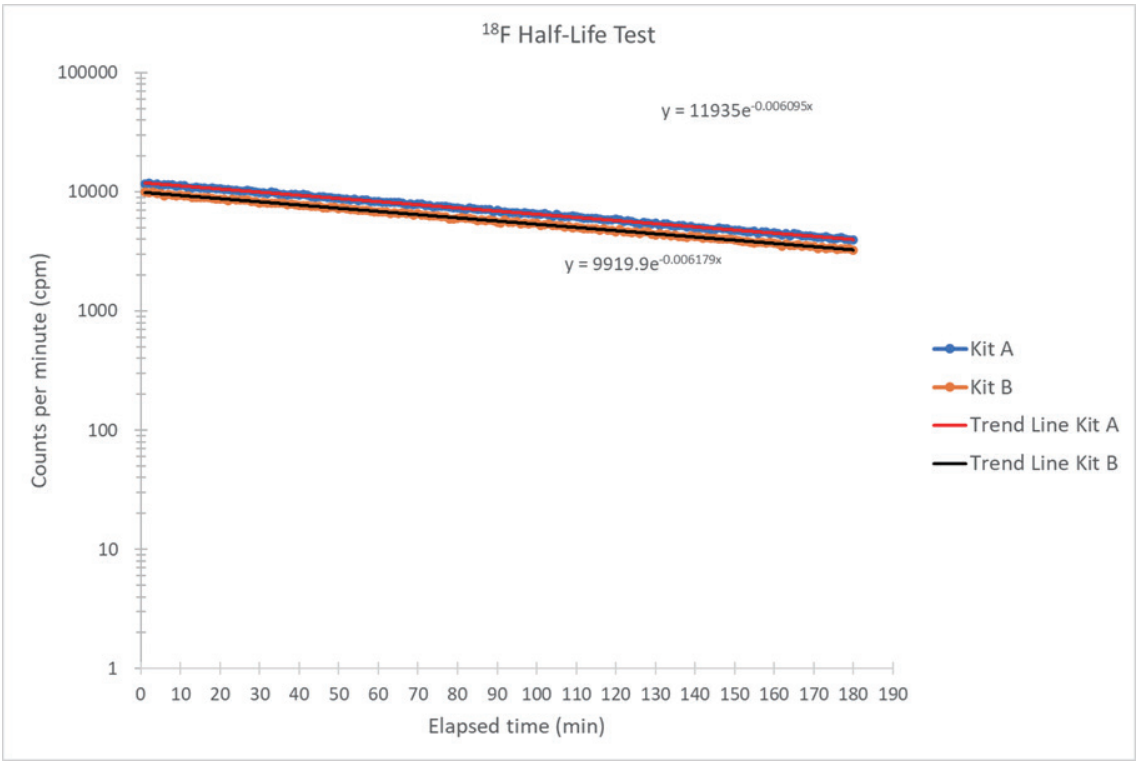

Figure 6. ^{18}F-FDG half-life counting results, Y-axis uses logarithmic scale.

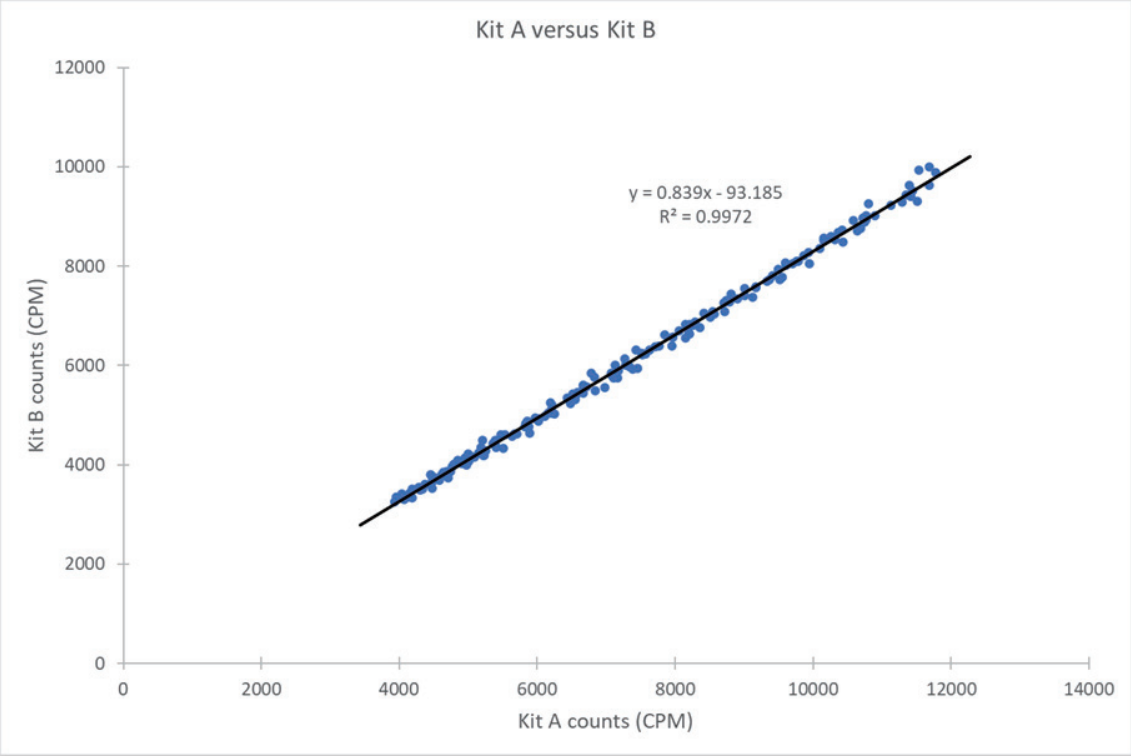

Figure 7. Correlation plot between the count rates measured by Kit A and Kit B. The solid line shows the result of a linear fit, with a slope equal to 0.839.

are then attracted toward the anode, while the heavier positive ions are drawn toward the cathode. As the electrons and ions move toward their respective electrodes, an electrical current is generated, causing a temporary drop in voltage between the anode and cathode. The counter detects this change in voltage and records it as a signal, thereby providing information about the presence of radiation[3-5, 11, 14].

A Geiger counter consists of a gas-filled tube. It is necessary to apply an appropriate operating voltage to trigger a complete discharge across the tube. The voltage range corresponding to the Geiger plateau is a critical operating region for GM tubes. When a GM tube is subjected to a constant radiation source and the applied voltage is gradually increased from zero, the resulting count rate exhibits a characteristic response curve. Within a specific voltage interval, known as the Geiger region, the count rate becomes relatively independent of the applied voltage, forming a plateau-referred to as the Geiger plateau. The characteristics of this plateau, including its voltage range and slope, vary depending on factors such as the tube's manufacturer, dimensions, and the type of fill gas used. The plateau slope is typically expressed as the percentage change in count rate per voltage range. To minimize fluctuations in detection efficiency due to voltage variations, GM tubes are typically operated with a regulated power supply set to the midpoint of the plateau[4]. This approach helps ensure stable performance by reducing sensitivity to minor voltage changes. The highest Geiger plateau slope of the J305 βγ tube employed in this investigation is 10% per 80 V, and its operating voltage range is 380 to 450 V.

The Geiger tube is a key component of the Geiger counter. Individual differences in the Geiger tube will affect the performance of the counter. To ensure accurate detection, the gas inside the GM tube is usually a mixture of inert gases such as helium, argon, or neon, along with a quenching gas like methane or halogens[4, 5, 11]. The quenching gas

prevents the occurrence of secondary ionization, which could lead to continuous discharge and incorrect readings. These quenching molecules degrade during operation, limiting the amount of pulses that a Geiger counter can monitor over its service life. [5] ◦ According to the manufacturer's data, the life of the J305βγ tube is approximately 10^9 pulses. According to the findings of this experiment, if it is just used for background radiation monitoring, at a counting rate of 15 to 20 CPM, the counter can run continuously for 60 years before approaching the limit of 10^9 pulses. The situation changes if the counter is always used in the presence of a strong radiation flux. The high number of ionization pulses may shorten the life of the Geiger counter.

The type and pressure of gas within a Geiger tube significantly impact its performance, affecting detection efficiency and overall operation[15, 16]. The gas's ionization properties and its ability to support avalanches determine how well the tube responds to ionizing radiation. The experiment used J305βγ tube GM tube, which has a glass sealed tube structure and the electrode penetrates the glass tube. Considering the probability of transmission damage and the tolerance of the production process, each tube has differences in glass thickness, internal gas ratio, and air pressure. The electronic components and circuit design of the two GM counter kits are identical. The primary distinction is that the installed GM tubes were produced in various years. From the results of this study, it can be seen that the counting rate of Kit B in each counting test is lower than that of Kit A. It is inferred that the difference in Geiger tubes is the main reason.

When two or more Geiger counters are arranged at a relatively small distance and operated under the same conditions, they can be used to compare the responses of different detectors and study the correlation between the radiation fluxes measured by each counter. If the counters are of the same type, it is usually expected that the number of counts per unit time should be comparable and the counts of each counter should be independent of each other within the statistical fluctuation range. However, over a long period of measurement, the radiation fluxes measured by individual counters may show some degree of correlation[5, 17, 18]. This study used the decay half-life characteristics of ^{18}F to simulate different conditions from high counting rate to low counting rate. The nuclear decay process follows: $N(t) = N_0 e^{-\lambda t}$. Among them, N is the number of atoms that have not decayed, and N_0 is the number of atoms at the initial time $t = 0$, which means that N decreases with the increase of time t, which is a process that satisfies exponential decay. The half-life ($t_{1/2}$), defined as $t_{1/2}=\ln 2/\lambda$, is the time it takes for N(t) to equal half of N_0[3, 17, 18]. Figure 5 illustrates that the counting results of the two counters are both exponential curves. An exponential curve will appear linear on a logarithmic scale. A logarithmic scale is a logarithmic transformation of the data so that the range of values can be presented more effectively, especially when the range of values varies greatly. Figure 6 confirms this phenomenon. The experimental results of the two counters are: Kit A fitting curve $y=11935e^{-0.006095x}$, and the half-life $t_{1/2}$ is converted to 113.71 minutes according to the half-life curve formula. Kit B fitting curve $y=9919.9e^{-0.006179x}$, and the half-life $t_{1/2}$ is converted to 112.17 minutes according to the half-life curve formula. The test results of the two sets of counter kits are very close to the physical half-life of ^{18}F-FDG, which is 109 minutes. The output of a usable ionizing radiation meter should be positively correlated with the intensity of the detected radiation. The results of this experiment confirm that the value of the Geiger counter is proportional to the intensity of the radiation. The relative relationship of the two Geiger counters in Figure 7 shows that the counting characteristics of the two counters are highly correlated, and the conversion factor can be set to achieve normalization.

As for the difference in the average count value of ^{137}Cs measured by the two counters, this may be due to the slight difference in detection efficiency between the counters. The main gamma ray photon energy of ^{137}Cs is 662 keV, which is higher than the 511 keV photons undergoes an annihilation reaction emitted by the radioisotope ^{18}F for the half-life test. Since the count rate response of GM tubes to photons of different energy scales shows a nonlinear relationship with the over-reading effect at low energies, the correction factors

calculated from the ^{18}F test may not be applicable to the experimental results of ^{137}Cs。 However, it should be noted that even a slight difference in the position of two adjacent detectors from the radioactive isotope may lead to different counting rates.

Conclusion

The experimental test results confirm that the counting response of the two Geiger-Müller counter kits exhibits a positive correlation under irradiation of different intensities of ionizing radiation. The Geiger-Müller counter kit is a device capable of performing basic ionizing radiation detection. Its applications include use in the fields of radiology and radiation protection-related education. However, it should be noted that individual variations in the counting efficiency of the kits may result in counting values that differ even under the same radiation intensity. Consequently, when conducting experiments involving multiple counters, appropriate adjustments should be made to account for these individual differences.

References

1. Ho, W., et al., *Radiation doses to staff in a nuclear medicine department.* JOURNAL-HONG KONG COLLEGE OF RADIOLOGISTS, 2002. 5: p. 24-28.
2. Shapiro, J., *Radiation protection: a guide for scientists, regulators, and physicians.* 2002: La Editorial, UPR.
3. Bailey, D.L., et al., *Nuclear Medicine Physics: A Handbook for Teachers and Students*. 2015: International Atomic Energy Agency.
4. McGregor, D. and J.K. Shultis, *Radiation Detection: Concepts, Methods, and Devices*. 2020: CRC Press.
5. Riggi, F., *Educational and Amateur Geiger Counter Experiments: 50+ Activities for Beginners and Beyond.* 2024: Springer Nature Switzerland.
6. Blanco, F., et al., *Geiger counters offer powerful way to teach detection methods.* Physics Education, 2006. 41(3): p. 204.
7. Goldader, J.D. and S. Choi, *An inexpensive cosmic ray detector for the classroom.* The Physics Teacher, 2010. 48(9): p. 594-597.
8. Remon, N.M., et al., *Build very simple design and cost effective Geiger-Muller counter.* Journal of Recent Advances in Applied Sciences (pISSN 0970-1990), 2024. 39(01).
9. Maw, A.M. and D.K.K.L. Thaw Tun Ko, *Arduino Based Geiger Muller Counter with SMS Alert System*.
10. Tysk, C., E. Brenner, and A. Olsson, *Construction of a Geiger counter: For cosmic radiation in near space conditions*. 2018.
11. Tackett Jr, F., et al., *Making a Geiger Muller radiation counter*. 2018.
12. Riggi, F., *Educational and Amateur Geiger Counter Experiments*.
13. Arcani, M., et al., *Transforming DIY Geiger Counter Kits into Muon Detectors for Education and Scientific Exploration*. Particles, 2024. 7(3): p. 603-622.
14. Silva, M.D.R., *Ionizing radiation detectors*. Evolution of Ionizing Radiation Research, 2015: p. 189-209.
15. Friedman, H., *Geiger counter tubes*. Proceedings of the IRE, 1949. 37(7): p. 791-808.
16. Arbutina, D. and A. Vasić-Milovanović, *Improving the geiger muller counter characteristics by optimizing the anode and cathode radius dimensions*. IEEE Transactions on Nuclear Science, 2020. 67(10): p. 2231-2237.
17. Poenaru, D.N. and W. Greiner, *Experimental techniques in nuclear physics*. 2011: Walter de Gruyter.
18. Visinelli, L., *Counting statistics using nuclear radiation*. 2014, ResearchGate.

評估兩款 Arduino 蓋格米勒計數器套件在不同輻射強度下的計數一致性

柴發順　江泰林　歐玲君　殷婉庭　陳柏勳　李正輝

新光吳火獅紀念醫院 正子造影中心

中文摘要

前言

蓋格計數器是一種用於偵測游離輻射的輻射偵測器。蓋格計數器因爲結構簡單、造價低廉、使用方便，被廣泛使用於核子物理、醫學及工業等領域中。本次實驗以兩台蓋格米勒計數器套件進行計數統計與半衰期計數測試，評估兩台計數器套件的計數性能一致性。

材料與方法

本實驗採用 Arduino 蓋格米勒計數器套件 (CAJOE，Model：GC-1602-NANO)，蓋格管型號 J305βγ。兩組套件分別標示爲 Kit A 及 Kit B 後以 USB 線連接電腦，利用 Tera Term 端口監視軟體紀錄 Arduino nano 電路板傳回的計數值。背景計數測試：無放射源情況下，每次計數 60 秒 (每分鐘計數值，CPM)，連續紀錄 240 次。計數統計測試：將蓋格米勒計數器套件固定在放射活性 114.26μCi 的 ^{137}Cs 放射源 1 公分處，連續紀錄 120 次。半衰期測試：將放射活性 6μCi 的 ^{18}F-FDG 固定在蓋格米勒計數器 1 公分處，紀錄 180 次，以擬合曲線推算半衰期。

結果

測試結果，Kit A 及 Kit B 的背景值計數平均值分別爲 19.33±4.16 CPM 和 15.69±3.82 CPM。^{137}Cs 放射源測試結果，Kit A 計數平均值 68777.88±190.39 CPM，Kit B 計數平均值 64898.40±271.90 CPM。半衰期測試結果，測量計數率曲線呈指數衰減曲線，Kit A 擬合曲線 $y=11935e^{-0.006095x}$，依照半衰期曲線公式換算半衰期 $t_{1/2}$=113.71 分鐘。Kit B 擬合曲線 $y=9919.9e^{-0.006179x}$，依照半衰期曲線公式換算半衰期 $t_{1/2}$=112.17 分鐘。兩組計數器套件測試結果皆與 ^{18}F-FDG 物理半衰期 109 分鐘極爲接近。

結論

本實驗測試結果證實蓋格米勒計數器套件可進行基本游離輻射偵測，可應用於放射線學或輻射防護相關教學。但由於套件的計數效能存在差異，相同輻射強度下的計數值會有差異。

關鍵字：蓋格米勒計數器、蓋格管、計數統計、半衰期、游離輻射

核醫技學誌 2025;22:11-20

接受日期：2025 年 6 月 19 日
通訊作者：柴發順
聯絡地址：台北市士林區文昌路 95 號新光吳火獅紀念醫院正子造影中心
電子郵件：T005629@ms.skh.org.tw

輻射防護：探討鉛衣汰換標準

解仲爲[1]　杜東峻[1]　陳怡勳[1]

戴德森醫療財團法人嘉義基督教醫院 核子醫學科[1]

摘要

對於從事放射工作的醫護人員而言，確保自身在作業過程中獲得足夠的防護至關重要。目前針對個人防護部分，鉛衣、鉛圍裙及鉛頸等都是防護的工具，然而，目前鉛衣是參考國外的汰換標準，未定義出適合本國輻射工作人員工作條件的汰換標準。因此本研究旨在通過對現有文獻的綜合分析及實際照射，以國內「游離輻射防護安全標準」規範，輻射工作人員有效劑量，加上參考目前國際輻射防護委員會103報告中對組織加權因子的修正，提出一套鉛衣評估標準，作爲醫療機構和輻射防護工作場所檢測與汰換鉛衣的依據。

關鍵詞：輻射安全、輻射劑量

核醫技學誌 2025;22:21-26

接受日期：2025 年 9 月 1 日
通訊作者：杜東峻
聯絡地址：嘉義市東區忠孝路 539 號
聯絡電話：05-276-5041，分機 7504
電子郵件：03587@cych..org.tw

1. 前言

在輻射防護領域中，工作人員的接受劑量被視爲重要的一部分，而減少散射輻射劑量主要有三個因素：暴露時間、與放射源的距離、輻射屏蔽[1,2]。對於輻射工作人員而言，鉛防護圍裙和鉛頸是介入醫護人員的標準防護設備[3,4]，它能夠提供物理屏蔽，有效降低穿透性輻射對人體的影響。然而，鉛衣隨著使用時間的增加及使用者的習慣，逐漸會出現裂痕、破洞或其它損壞[5]，這些破損會導致鉛衣的防護效果大幅降低，儘管所有工作人員都必須佩戴劑量計來監測輻射暴露[6]，但這監控方式並無法即時發現工作人員劑量異常問題。

目前，醫療機構及輻射工作場所對鉛衣的使用有一定的規範和管理，並且普遍要求進行鉛衣檢測確保其能夠提供足夠的輻射防護，防護罩需要定期進行射線照相檢查，如果檢查結果不合格，則會停用[7]。根據過去的文獻，大多數現有研究僅提及不同的檢測方法來發現鉛衣的裂痕或破洞[8]，但對於鉛衣在發生損壞後應採取何種不合格判定標準，卻缺乏明確的指引。

因此，本研究旨在通過對現有文獻的綜合分析及實際照射，以國內「游離輻射防護安全標準」規範，輻射工作人員每連續五年週期之有效劑量不得超過一百毫西弗，且任何單一年內之有效劑量不得超過五十毫西弗爲依據[9]，加上參考目前國際輻射防護委員會 103 報告中對組織加權因子的修正[10]，提出一套可操作的鉛衣評估標準，作爲醫療機構和輻射防護工作場所檢測與汰換鉛衣的依據。

2. 材料與方法

2.1 實測

根據臨床觀察，鉛衣破損可分爲裂痕與孔洞兩種類型，因此本研究將實驗分爲裂縫組與孔洞組。首先，將鉛衣裁切爲 10 × 10 cm^2 的鉛片，並以 X 光照射單片，篩

選出無摺痕且無損鉛片作爲實驗材料 (圖 1)。隨後將四片鉛片疊合，使其鉛當量達 0.25 mm²，再進一步模擬破損情況。裂縫組裂縫長度分別設爲 1、2、3、4、5 cm；孔洞則製作直徑爲 1、2、3、4、5 cm 的圓形孔洞 (圖 2)。本研究採用 GE「DISCOVERY MI GEN2」正子電腦斷層掃描儀進行照射，並使用 Scout view 照射，條件設定 80 kVp、50 mA，焦點至偵測器距離 (SID) 設定爲 50 公分。使用專用輻射劑量計「RaySafe X2 SOLO X-ray Measurement System」測量劑量率，單位爲 mGy/s，該儀器可測量 X 射線之 kVp、劑量及劑量率等參數。

在照射過程中，首先確認裂縫或孔洞位置與偵測器中心對齊，隨後進行全片掃描，掃描長度約爲 30 公分。每片樣本重複掃描 5 次，並取其平均值作爲測量結果。除此之外，亦進行空氣劑量及完整無破損鉛片之劑量率測量，並同樣以 mGy/s 爲單位記錄。

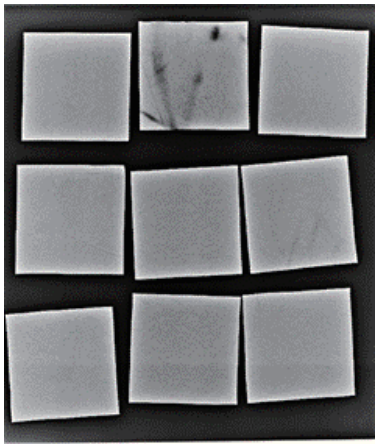

圖 1.　X 光照射下的鉛片

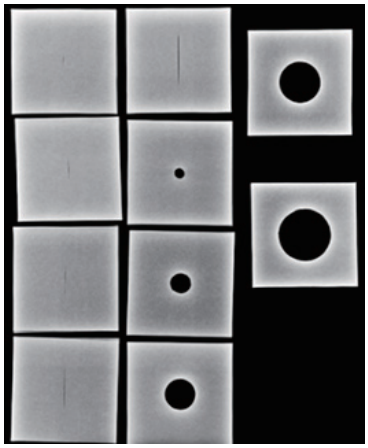

圖 2.　將鉛片裁切裂縫及孔洞

2.2 文獻

文獻部分採用歷年有提出明確汰換標準的研究做比較，本研究參考以下三篇：

一、由 Lambert 於 2001 年提出，以面積作爲汰換單位，汰換條件：鉛頸 11mm²、鉛衣 670 mm²、性腺區域 15 mm² [11]。

二、由 Stam 於 2008 年提出，以長度作爲汰換單位，汰換條件：鉛頸 19mm 裂縫、鉛衣 270 mm、性腺區域 87 mm[12]。

三、由 Joan 於 2023 年提出，以面積作爲汰換單位，汰換條件：鉛頸 279mm²、鉛衣 370 mm²、性腺區域 37 mm² [13]。

值得注意的是，Lambert 與 Stam 的研究中參考 ICRP 60 號報告提出的組織加權因數；Joan 與本篇的研究中參考 ICRP 103 號報告提出的組織加權因數。

與過往文獻所測得的劑量不同，本研究所偵測到的數值單位爲劑量率，因此需再考量輻射工作人員的職業暴露時間。本研究以心導管醫師爲例，因爲他們藉受到輻射曝露的時間相較於其他單位得輻射工作人員更久 [14]，依據 Dilschad Murat 研究中所提出心導管工作人員曝露時間 [15]，約略可計算心導管醫師一年會接收到曝露的時間爲 8000 分鐘。

3. 結果

每個鉛片進行平面掃描，包含空氣與完整無破損鉛片，重複 5 次後紀錄並平均，並區分爲裂縫及孔洞，表 1 爲測量的平均結果，我們以曲線圖表示並劃出趨勢線 (圖 3、圖 4)。

依據游離輻射防護安全標準與趨勢線計算，可得出汰換標準：在裂縫方面，鉛頸汰換條件爲 10.89 cm 裂縫、鉛衣 12.79 cm、性腺區域 11.72 cm；使用影像將裂縫長度計算爲面積 [16]，可得出：鉛頸汰換條件爲 8.3mm² 裂縫、鉛衣 11.45 mm²、性腺區域 9.61 mm²。

在孔洞方面，可以發現在直徑 1 公分的孔洞劑量率已與空氣的劑量率相近，從穿透率來看達到 96%，因此認定有破損 1 公分以上的孔洞無任何防護效果，不列入計算。

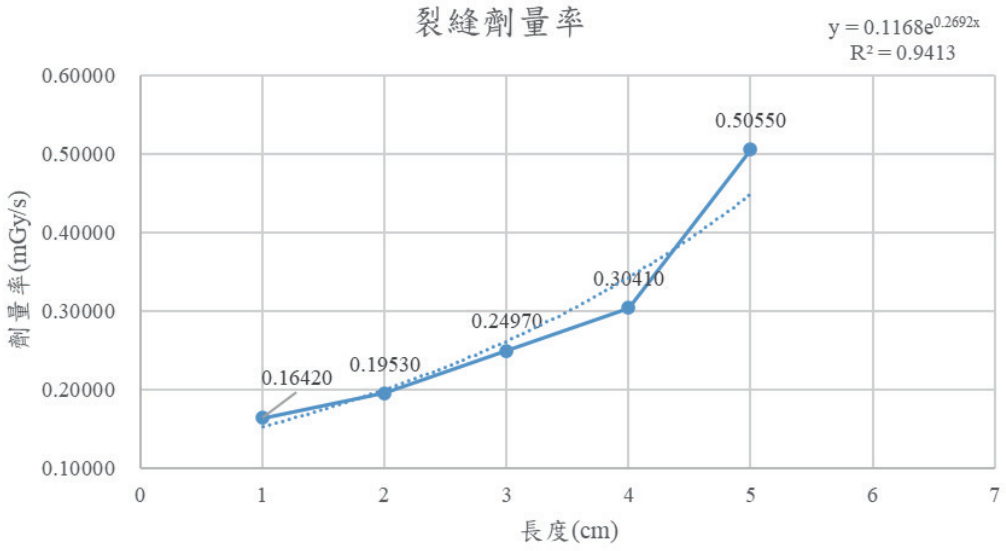

圖 3.　裂縫測量平均結果曲線圖並記錄趨勢線

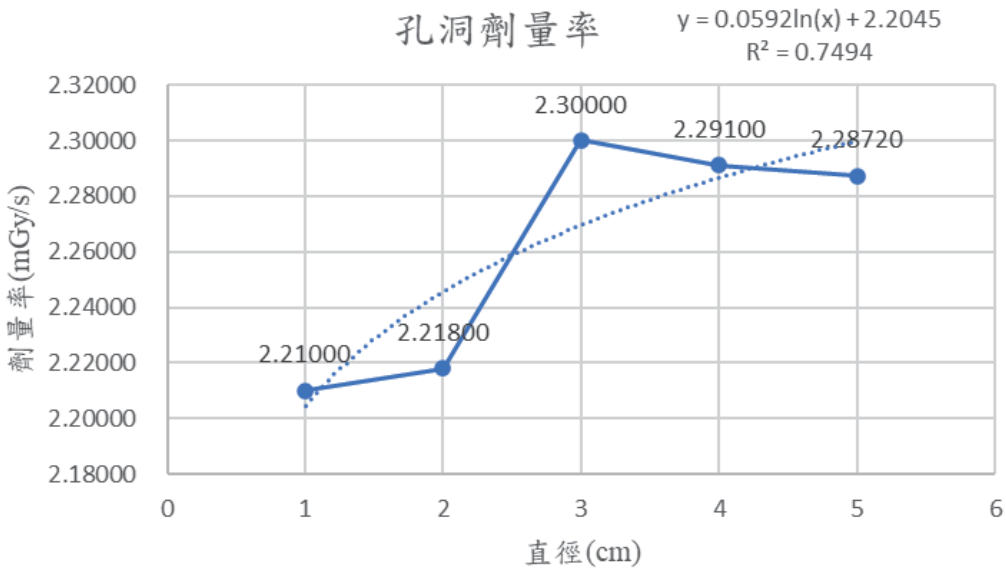

圖 4.　孔洞測量平均結果曲線圖並記錄趨勢線

表一 裂縫與孔洞的劑量率測量平均值

裂縫長度 (cm)	空氣	無破損	1	2	3	4	5
劑量率 (mGy/s)	2.3050	0.10240	0.16420	0.19530	0.24970	0.30410	0.50550
孔洞直徑 (cm)	空氣	無破損	1	2	3	4	5
劑量率 (mGy/s)	2.3050	0.10240	2.21000	2.21800	2.22000	2.21660	2.22150

4. 討論

鉛衣作爲輻射工作人員輻射防護的第一道防線，本研究採取較嚴格的評估方式，將損壞型態區分爲裂縫與孔洞。從結果表 1 可見，相同尺寸的裂縫及孔洞所造成的額外劑量率差異極大，其中直徑達 1 公分以上的孔洞，其劑量率已接近空氣中的劑量率，等同於鉛衣或鉛頸失去防護效果。因此後續計算上以及與文獻的比較中，孔洞不列入討論。

與 Lambert 條件比較，他的鉛頸與性腺區域汰換條件較爲嚴格，鉛衣則較爲寬鬆，但三項條件與本研究相比面積還是偏大，其原因可推測本研究只比較裂縫，裂縫面積推算會遠比孔洞更小。另外，Lambert 所參考的組織加權因數是 ICRP 60 號報告，而本研究則參考 ICRP 103 號報告，並且 Lambert 的汰換條件中有加入成本的概念，即機構願意投入多少資金來換取輻射防護效果 [11]。在其研究中，鉛頸屬於相對更換成本較低的裝備，因此可以採用更嚴格的標準進行汰換。。

與 Stam 條件比較，可以發現本研究在鉛頸與性線部分的汰換條件明顯寬鬆。在 Stam 的研究中，有提出一條將裂縫長度計算爲面積的公式 $2L=2\pi r$(L 爲裂縫長度，r 爲半徑)[12]，當我們將公式與影像計算出的面積做比較，可發現 Stam 的公式明顯高估裂縫產生的面積，造成更高的洩漏劑量，因此他的汰換條件較爲嚴格。

與 Joan 條件比較，他的整體汰換條件較爲寬鬆，雖然與本研究相同，都是參考 ICRP 103 號報告提出的組織加權因數，但與 Lambert 相同，Joan 的公式汰換條件使用的是破損孔洞，計算中裂縫的推算面積更小，因此汰換條件會更加嚴格。另外在他的公式中，會考量受曝露區最敏感器官或組織的截面積，也就是參考最敏感器官或組織在整體受曝露區的比例 [13]，進而加入公式中做計算，因此在最大允許面積上會與本研究有所不同。

5. 結論

本研究希望在兼顧更換鉛衣成本的前提下，以實際測量的方式提出一項新的鉛衣汰換標準，與歷年的文獻皆有些許差異，主要原因爲本次研究只計算裂縫，換算成面積後會與文獻有較大差異，其次在於計算模式不同，以及各地區的輻射劑量限值差異，未來期許可以提出一項能匹配各地區的汰換公式，也能將孔洞及裂縫以更小的面積做實測，完善出一套特地區皆能使用的鉛衣汰換條件。

6. 參考文獻

1. Fishman SM, Smith H, et al. Radiation safety in pain medicine. Reg Anesth Pain Med. 2002 May-Jun;27(3):296-305.
2. Sarah Smith, Jie Zhang, et al. Protective Apparel Integrity Inspection Where We Are and What We Need. J Am Coll Radiol. 2016 Oct;13(10):1223-1226.
3. Park PE, Park JM, et al. Radiation safety and education in the applicants of the final test for the expert of pain medicine. Korean J Pain. 2012 Jan;25(1):16-21.
4. Kim C, Vasaiwala S, et al. Radiation safety among cardiology fellows. Am J Cardiol. 2010; 106:125–128.
5. Linda Wie Bjørkås, Sandra Blø, et al. Quality of radiation protection aprons and quality control routines at different diagnostic imaging modalities. Radiography Open.2020 Dec;6(1):64-74.
6. Durán A, Hian SK, et al.Recommendations for occupational radiation protection in interventional cardiology. Catheter Cardiovasc Interv. 2013 Jul 1;82(1):29-42.
7. Clements J., Moirano J., et al.Best practices for evaluating and tracking protective garments. J Am Coll Radiol. 2015 May;12(5):531-2.

8. Orhan Oyar, Arzu Kışlalıoğlu. How protective are the lead aprons we use against ionizing radiation? Diagn Interv Radiol . 2012 Mar-Apr;18(2):147-52.
9. Safety Standards for Protection against Ionizing Radiation. https://law.moj.gov.tw/ENG/LawClass/LawAll.aspx?pcode=J0160004.
(參考時間 :2025/08/07，13:00).
10. J. Valentin et al. The 2007 Recommendations of the International Commission on Radiological Protection. ICRP Publication 103.
11. Kent Lambert and Tara McKeon. Inspection of Lead Aprons: Criteria for Rejection. Health Phys. 2001 May;80(5 Suppl):S67-9.
12. W. Stam and M. Pillay. Inspection of Lead Aprons: A Practical Rejection Model. Health Phys. 2008 Aug:95 Suppl 2:S133-6..
13. Joan M Brewer, Kevin Hammerstrom, et al. Reassessing lead protective garment assessment using ICRP 103 tissue weighting factors. J Radiol Prot. 2023 Jul 10;43(3)
14. Sylvia Marie R. Biso, Mladen I. Vidovich. Radiation protection in the cardiac catheterization laboratory. J Thorac Dis. 2020 Apr;12(4):1648-1655.
15. Dilschad Murat, Christian Wilken-Tergau, et al. Effects of Real-Time Dosimetry on Staff Radiation Exposure in the Cardiac Catheterization Laboratory. J Invasive Cardiol. 2021 May;33(5):E337-E341.
16. Chun Liu, Chao-Sheng Tang, et al. Automatic quantification of crack patterns by image processing. Comput. Geosci.2013 Aug;57:77-80.

7. 致謝

本研究部分經費承蒙「戴德森醫療財團法人嘉義基督教醫院研究計畫經費補助 (R111-32)」補助，使我能順利完成研究工作。

Radiation Protection: An Evaluation of Replacement Criteria for Lead Aprons

Jung-Wei Hsieh[1], Dom-Gene Tu[1], Yi-Hsun Chen[1]

[1]*Department of Nuclear Medicine, Ditmanson Medical Foundation Chia-Yi Christian Hospital*

Abstract

or medical personnel engaged in radiological procedures, ensuring adequate personal protection during operations is crucial.

Currently, protective tools such as lead aprons, lead skirts, and thyroid shields are commonly used. However, existing replacement criteria for lead aprons are based primarily on foreign guidelines, and there is still no standard specifically tailored to the working conditions of radiation workers in Taiwan.

This study aims to establish an evaluation framework for lead apron replacement by conducting a comprehensive literature review and performing practical irradiation tests. The framework is developed in accordance with the domestic Safety Standards for Protection Against Ionizing Radiation and the effective dose limits for radiation workers, while also incorporating the updated tissue-weighting factors from the International Commission on Radiological Protection (ICRP) Publication 103. The proposed evaluation standard is intended to serve as a reference for medical institutions and radiation-protection facilities in the testing and replacement of lead aprons.

Keywords: Lead Apron, Radiation Safety

J Nucl Med Tech 2025;22:21-26

Received 2025/9/1
Corresponding author: Dom-Gene Tu
Address: Ditmanson Medical Foundation Chia-Yi Christian Hospital, Chiayi 600, Taiwan; No. 539, Zhongxiao Rd., East Dist., Chiayi 600, Taiwan
Tel: 05-276-5041#7504; E-mail: 03587@cych..org.tw

Using Virtual Reality (VR) for Simulation Exercises of Radiation Hazard Injuries

Yao-Wen Chen[1], Chih-Wei Chang[1], Jui-Yin Kung[1], Jing-Wei Hou[1], Tzu-Chiang Chiang[2], Shih -Chuan Tsai[1]

[1]*Department of Nuclear Medicine, Taichung Veterans General Hospital, Taichung, Taiwan, R.O.C.*
[2]*Department Of Information Management, Tunghai university, Taichung, Taiwan, R.O.C.*

Abstract

When radiation disasters (radiation pollution from nuclear power plants, radiological dirty bombs, etc.) occur, patients will be sent to the responsible district hospitals. The designated personnel at these hospitals will be responsible for receiving and treating patients suffering from radiation injuries. The incidence of such accidents is extremely low. If the personnel responsible for medical treatment and radiation protection are not routinely trained, they are likely to cause injuries due to their unfamiliarity with the relevant treatment procedures when an accident occurs suddenly. In this study, we aim to conduct simulation exercises via virtual reality (VR) to increase the number of exercises and reduce costs.

Keywords: radiation hazard injuries; virtual reality (VR)

J Nucl Med Tech 2025;22:27-34

BACKGROUND

With the advancement of science and technology and the development of economy, the application of radiation is becoming more and more extensive.

Radiation-related accidents may be induced due to improper use, human negligence, equipment malfunction, or natural disasters. When radiation disasters, such as nuclear accidents, overseas radiation disasters, and presence of radiological dirty bombs, occur, people around may experience radiation contamination and injuries. If such patients are not attended properly, there will be a high risk of residual radiation and spread of radiation contamination, leading to unexpected harm. In order to provide proper medical care for patients suffering from radiation damage in the event of a radiation disaster, government agencies, such as Atomic Energy Council, fire departments, and the hospitals responsible for radiation disasters invest a lot of labor, economic, and material resources every year in organizing relevant workshops or practical drills for response personnel on performing treatment of radiation injuries to reinforce the knowledge and competency required. However, classroom teaching cannot provide practical practices, and actual drills consume labor, economic, and material resources to such level that the effect is disproportionate to the cost. Therefore, how to enable medical and radiation protection personnel in different departments to conduct drills anytime and anywhere without being limited by time and space and to improve related personnel on the familiarity with the disaster response process is a dilemma to be overcome urgently.

Received 2025/10/14
Corresponding author: Yao-Wen Chen
Address: 1650 Taiwan Boulevard Sect. 4, Taichung, Taiwan 407219, ROC
Tel: 04-23592525#4820
E-mail: jywen@vghtc.gov.tw.tw

INTRODUCTION

Disaster drills can be designed to completion according to the evaluation method 1. Action Plan Discussion 2. Tabletop Exercise 3. Full-Scale Exercise {1,2,3}

The best way to improve the familiarity and experience of the drillers is the Full-Scale Exercise, which also requires the most resources. Among them, medical staff spend a lot of time participating in classroom trainings, and only a few can participate in drills. In order to reflect the situation of avoiding the spread of radiation contamination, a considerable number of general affairs personnel must be deployed to control the traffic flows, cover affected areas with waterproof pads on the day of the exercise, and occupy the space of the emergency department to reduce the number of patients admitted to the emergency department. With the rise of advanced technologies, Virtual Reality has become one of the options for disaster response drills. VR can build the environment and situation you imagine, especially those costly scenes in reality. As literatures also show, that is a potential advantage of VR, given that many participants can use a training computer asynchronously over a long time period, instead of gathering a limited number of staff for a limited number of training sessions {4.5}. Overall, VR can be an effective training tool and has also been proven to be a cost-effective medium. The high upfront cost of VR can quickly become long-term cost saving, while the number of employees trained increases and training is repeated over time{6.7}. There have been many studies on the use of VR in disaster drills such as fires and earthquakes, all of which have achieved good results {8-12}, but there are very few studies on the use of VR in handling patients with radiation injuries. This study aims to establish a VR scene of radiation disasters for Full-Scale Exercise to improve the situation where medical staff are limited by space and time.

MATERIALS and METHODS

In this section, the main design choices were illustrated, followed by the description of the game's storyline.

A. System design

In this study, a VR system for radiation hazard Injuries drill was developed, providing repetitive practices unrestricted to venue and time for response personnel to independently obtain knowledge and familiarity from drills of different scenarios.

a. System Function and Scenarios

Handling of patients with radiation injuries requires teamwork, which involves physicians, nurses, and radiation protection personnel. Based on scenarios of radiation injuries drill, a patients with contaminated wounds is sent in bed for treatment in our hospital, the response site of which is the emergency department. Drill site is divided into three areas. In each area are options of roles and corresponding actions. Those under training can choose the role in the same area for practice.

b. Production of Script and Exercise Process

According to scenarios of radiation injuries, exercise scenes were set as 1. Emergency triage area 2. Decontamination area 3. Evacuation area (Figure 1). The patient is sent to different areas for corresponding processes. Roles of response personnel (Figure 2) to be selected in each area are as follows:

(1) Emergency triage area: emergency physician, emergency nurse, emergency radiation protection personnel, and control area radiation protection personnel
(2) Decontamination area: decontamination physician, decontamination nurse, decontamination radiation protection personnel.
(3) Evacuation area: evacuation physician
(4) Tasks corresponding to the roles include medical decontamination, specimen collection, radiation detection, data reporting, and basic measurement.

B. Use of VR Tools and Construction of Drill Scenes

The study was based on the photo shot on-site of an actual radiation injury drill (Figure 3); via Sketchup, the virtual drill site and character modules were established (Figure 4, 3D module reconstruction). Data were imported into UNITY game engine to establish relevant responsible personnel modules and duties. Virtual drills were conducted based on different processing procedure of different duties. Oculus Quest 2 was used by response personnel to conduct drills.

Figure 1. scene selection

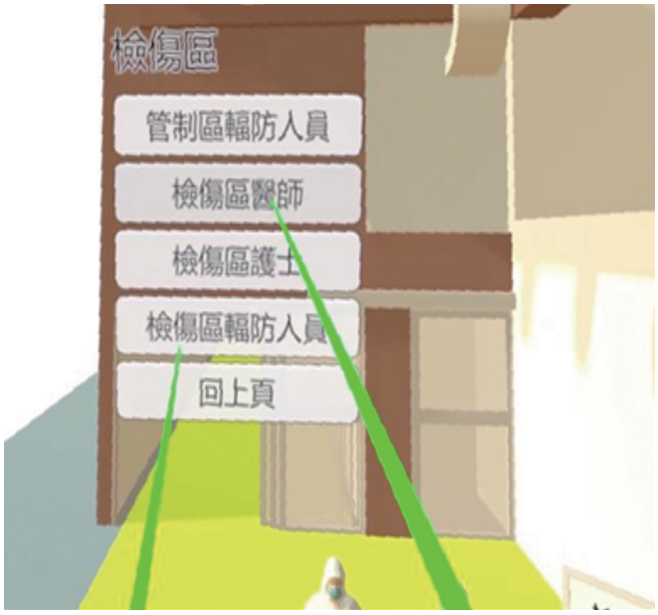

Figure 1. character selection

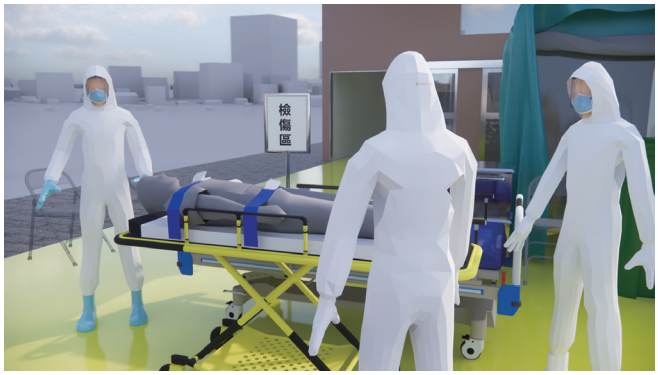

Figure 3. photo shot on-site with characters and scripts

Figure 4. Virtual venue

(1) Sketchup software: used for construction of 3D environment, modeling floor plan and hospital equipment for the reproduction in VR.

(2) Unity software: a game-developing engine. The supporting library imports the modeling done in the previous step into the engine and writes logic so that each trainee needs to complete the corresponding task.

(3) Oculus Quest 2: Head-mounted device, using the four front-facing cameras to locate the coordination in the real world without connecting to a computer or plugged in with a cable, has the ability to process apps itself.

(4) Task reminder: There are subtitles and sounds during task execution to let the trainees know the next step clearly.

C. VR Training Questionnaire and Feedbacks

After the VR construction was completed, 20 medical staff aged between 24 and 55 were invited to perform the testing and give feedbacks according to the process designed (Figure 5~7). 10 radiation protection personnel, 6 nurses, and 4 physicians (4 of the radiation protection personnel have experience in participating in radiation injury drills, and the rest have no experience) answered the questionnaire system after the experience. Five-level evaluation Likert scale and a free-form questionnaire were included. These questions are shown in Table 1:

Figure 5. VR training screen

Figure 6. VR training screen

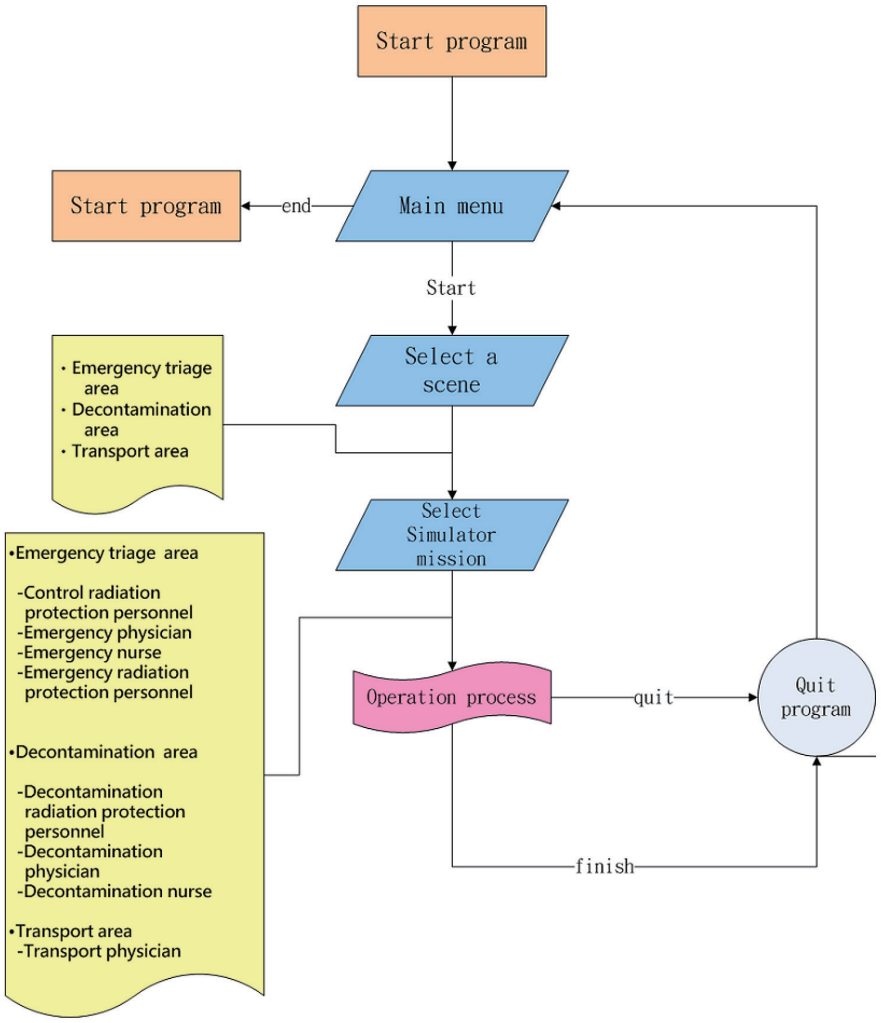

Figure 7. Process deisgned

Table 2. Statements assessed in the questionnaire.

Aspect	Strongly Agree	Agree	Neutral	Disagree Strongly	Disagree
Knowing the character's works(after VR drill)	○	○	○	○	○
Realistic VR training environment	○	○	○	○	○
The VR walkthrough process is good	○	○	○	○	○
VR instruction is clear	○	○	○	○	○
Feeling unwell after VR drill	○	○	○	○	○
If you have any comments about this disaster excrcises, please describe :					

Results and Discussion

After the completion of the platform construction, 20 medical staff experienced it and gave feedbacks (Fig 8). It was found that after performing the VR exercise, for the option of feeling unwell after performing VR drill for a period of time, percentage of strongly agree and agree was 40% for radiation protection personnel, 25% for physicians, 17% and 33% for nurses. For understanding of the character's duties (after VR drill), radiation protection personnel strongly agree with 100%, while physicians and nurses agree and strongly agree with 50%, respectively. For the question, VR guiding is clear, radiation protection personnel strongly agree with 100%, 50% for physicians, 67% and 33% for nurses. The content of the free-form questionnaire inferred that people would feel dizzy during the transition of scene. Some participants commented that there should be more task options for practice, even automatic assessments with scores. A small number of participants suggest simultaneous online practice.

In this study, virtual reality (VR) was used to construct radiation disaster drill scenarios, and medical staff performed drills with different scripts and scenarios, establishing knowledge and correct actions in the immersive experience. During the entire research and development process of importing scripts, it was found that the fineness of character modeling (skeleton) would affect the production of the Unity game engine. The simpler the skeleton function was, the less coordinately the character model moved; on the contrary, with good skeleton function, movements of character model would be more lifelike, but the cost would be relatively high. As it is the norm that there's change of duty for response personnel and difficulty to conduct regular drills, the effectiveness was unable to evaluated via questionnaires of pre-testing and post-testing, meanwhile, there was no design to show scores immediately after the exercise. From the results of the VR platform exercise built in this research, after the exercise, the medical staff have a clear understanding of the actions to be performed by their role in the exercise. However, the physical discomfort generated after performing VR for a period of time was caused by dizziness in the head because the research scene was built in a 1:1 ratio. Movements were required in some of the scenes, which caused physical discomfort; for example, radiation detection required participants to walk around in the script to measure patients and ambulances. In the future, in terms of movement, teleportation may be considered to reduce discomfort, but the relative fidelity may not be enough. The reason for the relatively less positive feedback on the realization of VR rehearsal environment and good rehearsal interaction process was that the script of this study was a

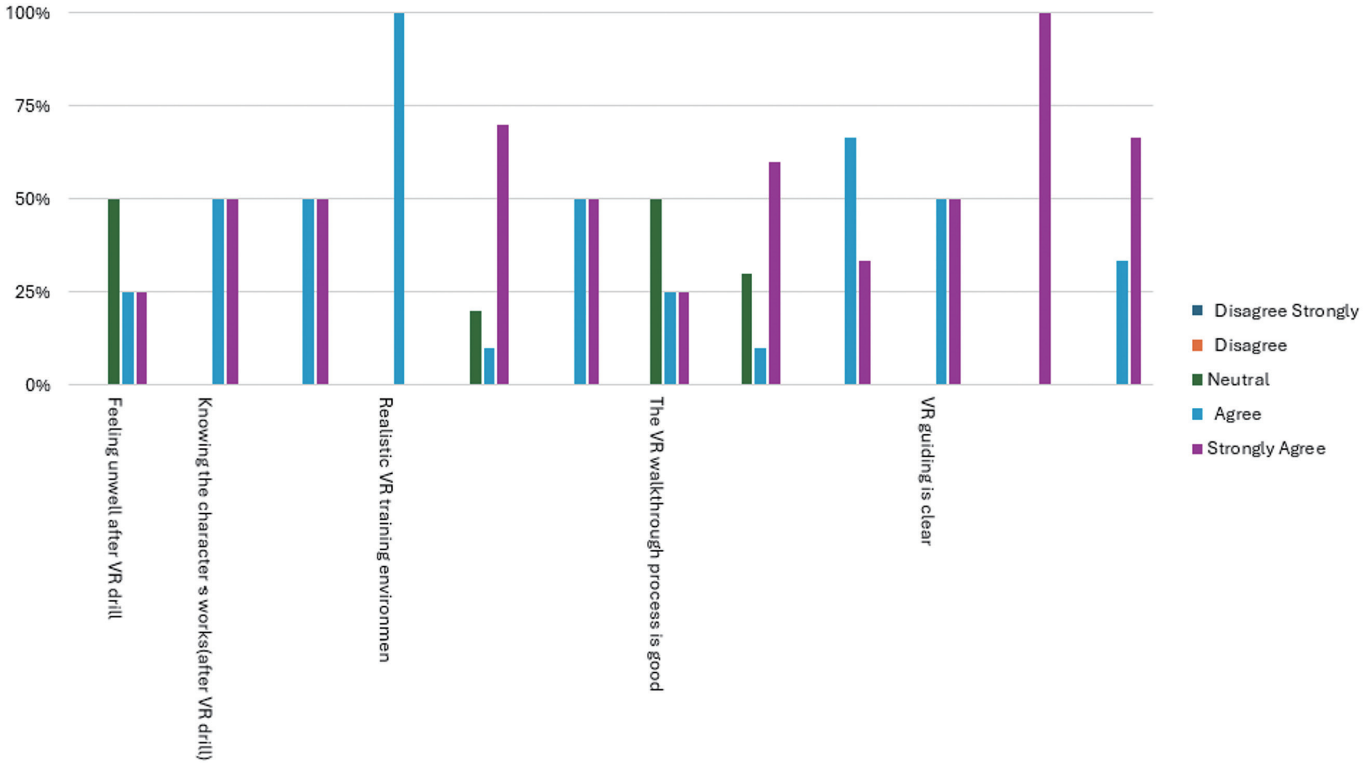

Figure 8. Questionnaire feedback.

stand-alone mode and the character skeleton function was relatively basic, unable to produce finer movements during drills.

CONCLUSION

In this study, environment and character modeling are relatively basic, the finished product can be used as an experience lesson plan for radiation hazard injuries. It is indicated in references that the decay of knowledge begins approximately 3 months after an actual drill; annual training may just not be enough.{6} VR can assist in repetitive training environments, and it can be combined with Full-Scale Exercise to achieve the best results. In the future, our goal is to continuously upgrade the version, strengthen the fine movement of characters, and add a scoring system to evaluate actions done in VR exercise. Correctness of actions can be presented immediately after the exercise. If a person fails the exercise, do-overs would be requested until qualifying score is met. Also, accommodation of multiple participants performing drills online simultaneously is to be added as well as a new process of washing and decontaminating patients without wounds with water to achieve the effect of an actual drill.

REFERENCES

1. Radiation Disaster Prevention and Response Plan (Nuclear Safety Commission)
2. The Medical Aspects of Radiation Incidents
3. The Ionizing Radiation Accident Emergency Response Plan includes specific protocols for decontamination (Taichung Veterans General Hospital, personal communication, October 14, 2025).
4. Rahouti, A., Salze, G., Lovreglio, R., & Datoussaïd, S. (2017). An immersive serious game for firefighting and evacuation training in healthcare facilities. International Journal of Computer and Information Engineering, 11(9), 1088-1094.

5. Lu, X., Yang, Z., Xu, Z., & Xiong, C. (2020). Scenario simulation of indoor post-earthquake fire rescue based on building information model and virtual reality. Advances in Engineering Software, 143, 102792.
6. Farra, S. L., Gneuhs, M., Hodgson, E., Kawosa, B., Miller, E. T., Simon, A., Timm, N., & Hausfeld, J. (2019). Comparative cost of virtual reality training and live exercises for training hospital workers for evacuation. Computers, informatics, nursing: CIN, 37(9), 446.
7. Ren, A., Chen, C., Shi, J., & Zou, L. (2006). Application Of Virtual Reality Technology To Evacuation Simulation In Fire Disaster. CGVR,
8. Ooi, S., Kikuchi, A., Goto, T., & Sano, M. (2021). Development and Verification of Mixed Disaster Training System in Virtual Reality Based on Experience Learning. 2021 10th International Conference on Educational and Information Technology (ICEIT),
9. Feng, Z., González, V. A., Amor, R., Spearpoint, M., Thomas, J., Sacks, R., Lovreglio, R., & Cabrera-Guerrero, G. (2020). An immersive virtual reality serious game to enhance earthquake behavioral responses and post-earthquake evacuation preparedness in buildings. Advanced Engineering Informatics, 45, 101118.
10. Krishnan, R. R., Sushil, S., Hrishikesh, R., Devadas, S., Ganesh, A., & Narayanan, G. (2019). A novel virtual reality game for disaster management applications. 2019 International Conference on Communication and Signal Processing (ICCSP),
11. Silva, J. F., Almeida, J. E., Rossetti, R. J., & Coelho, A. L. (2013). A serious game for EVAcuation training. 2013 IEEE 2nd International Conference on Serious Games and Applications for Health (SeGAH),
12. Lovreglio, R., Gonzalez, V., Feng, Z., Amor, R., Spearpoint, M., Thomas, J., Trotter, M., & Sacks, R. (2018). Prototyping virtual reality serious games for building earthquake preparedness: The Auckland City Hospital case study. Advanced Engineering Informatics, 38, 670-682.

使用虛擬實境 (VR) 進行輻災傷患模擬演練應用

陳耀文[1] 張志維[1] 龔瑞英[1] 侯景維[1] 姜自強[2] 蔡世傳[1]

[1]臺中榮民總醫院 核子醫學科
[2]東海大學 資訊管理學系

中文摘要

當發生輻射災害 (例如：核電廠輻射工作人員污然事件或輻射髒彈事件…) 時，傷患依發生地點送往責任分區醫院，輻射，這些醫院將有專人負責接收和治療輻射傷害病患。我們希望通過虛擬現實 (VR) 進行模擬演練，增加演練次數，降低實兵演練成本。

研究方法

本研究使用 Sketchup 軟體來建置 3D 演練環境 (本院實兵演練場地) 與人物建模，匯入遊戲開發引擎 Unity 製作 1. 檢傷區、2. 除汙區、3. 後送區等醫師、護理師、輻防人員角色與腳本，透過頭戴式裝置 Oculus Quest 2 讓參與應變人員透過不同腳本與場景方式演練。我們邀請了 20 人使用 VR 平台，其中輻射防護人員 10 人，護士 6 人，醫師 4 人。 這些人中，有 4 名輻射防護人員參加實兵演練經驗，其它人沒有。 每位參與者在使用 VR 後都完成了一份問卷調查。

結果與討論

從演練結果來看，醫護人員對演練中角色所要執行的操作有清楚的理解。然而，由於研究場景是 1:1 比例搭建的，在進行一段時間的 VR 體驗後，會產生頭部眩暈感等身體不適感。另外由於緊急應變人員職責變動較爲頻繁，且演練難以定期進行，因此無法透過 VR 演練前測和實兵演練後測的問卷進行效果評估，也沒有演練結束後立即顯示評分的設計。

結論

本研究的環境與角色建模較爲基礎，成品可以作爲輻射傷害的體驗教案。未來我們的目標是不斷升級版本，強化角色的精細動作，並增加評分系統來評估 VR 演練中的動作。

關鍵字：輻傷演練；虛擬實境

核醫技學誌 2025;22:27-34

接受日期：2025 年 10 月 14 日
通訊作者：陳耀文
聯絡地址：407219 台中市西屯區台灣大道四段 1650 號 核子醫學科
通訊電話：04-23592525#4820
電子郵件：jywen@vghtc.gov.tw.tw

建置臺灣醫事放射職類核子醫學領域里程碑

龔瑞英[1,2]　陳惠萍[3*]　許幼青[4]　陳建榮[5]　張婉柔[6]　張嘉容[7]

[1] 臺中榮民總醫院 核子醫學科
[2] 中臺科技大學 醫學影像暨放射科學系
[3] 臺東基督教醫院 核子醫學科
[4] 佛教慈濟醫療財團法人大林慈濟醫院 核子醫學科
[5] 國立臺灣大學醫學院附設醫院 核子醫學部
[6] 國立臺灣大學醫學院附設醫院癌醫中心分院 核子醫學部
[7] 臺北榮民總醫院 核子醫學部
[*] 通訊作者

摘要

為推動以勝任能力為導向的醫學教育 (Competency-Based Medical Education; CBME)，台灣醫事放射師全國聯合會 (Taiwan Association of Medical Radiation Technologists; TAMRT) 已完成放射師五大核心能力與 14 項可信賴專業活動 (Entrustable Professional Activities, EPAs) 的建置。本研究旨在運用焦點團體法 (Focus Group Method) 建構臺灣核子醫學里程碑共識，以完善 CBME 評估工具。

本次「放射核醫領域醫學里程碑共識」擬針對五大核心能力之次核心能力各項里程碑進行專家共識，初步由專家小組針對各次核心能力撰寫各項學習里程碑，於 2024 年 3 月進行全國問卷普查，並於 2024 年 3 月 30 日舉行全國核醫專家團隊共識，邀請 28 位來自 (準) 醫學中心、區域醫院的核子醫學領域醫學教育專家參與。首先由醫學教育專家進行里程碑文獻回顧與共識教育訓練，接著進行焦點團體討論及表決。本次團隊共識使用「焦點團體法」(Focus Group Method) 進行里程碑的討論及表決，共計進行 171 項次的團體表決，表決後 143 項次議案維持原案、28 項次議案修改。最後，使用修正式德菲法 (Modified Delphi Method, MDM) 進行共識程度投票，結果顯示共識程度為 4.93 分，完成 125 項臺灣核子醫學里程碑的建置。

本研究運用焦點團體法建構臺灣核子醫學里程碑共識，為 CBME 評估工具的建置奠定基礎。未來可持續追蹤里程碑的應用成效，並適時調整與精進。

關鍵詞：勝任能力為導向的醫學教育 (CBME)、里程碑、焦點團體法、修正式德菲法 (MDM)

核醫技學誌 2025;22:35-40

接受日期：2025 年 11 月 10 日
通訊作者：陳惠萍
聯絡地址：台東縣台東市開封街 350 號
聯絡電話：089-960888#8172；傳真：089-341729
電子郵件：a13026@tch.org.tw

前言

勝任能力為導向的醫學教育 (Competency-Based Medical Education, CBME) 已成為全球醫學教育的重要趨勢，美國畢業後醫學教育評鑑委員會 (Accreditation Council for Graduate Medical. Education, ACGME)、加拿大住院醫師教育認證聯盟 (Canadian Residency Accreditation Consortium) 與歐洲多國醫療教育體系皆已建立完善的 CBME 架構，並持續精進其訓練與評估機制 [1,2]。相較於傳統醫學教育以訓練時數或年資作為學習成果判定標準，CBME 更強調學習者是否眞正達成預期能力，採「以學習成果為中心」的模式，並重視觀察、回饋與可驗證的能力表現 [3]。

在此框架下，可信賴專業活動 (Entrustable Professional Activities, EPAs) 與里程碑 (Milestones) 已成為評估臨床能力的重要工具。EPAs 著重於評估學員是否能被信任獨立執行特定臨床任務，而里程碑則提供各

項能力的發展進程，描述學員從初學者到獨立執行者的逐步成長 [3]。里程碑的概念奠基於德雷福斯技能獲得模型 (Dreyfus model of skill acquisition)，主張臨床能力如同人類發展般具明確階段性，其行爲表現可被定義與觀察 [4]。「里程碑」這個名詞首次在醫學教育領域提出時，指的是在某一特定能力訓練過程中設定數個關鍵性指標，用來確定學習者是否能達到預定的階段目標 [5]。

在國際間，里程碑已成爲建構 CBME 的核心工具。以美國 ACGME 爲例，住院醫師訓練過去因院所差異而「做法不一、標準不一致」，導致學習成果難以比較與追蹤。而里程碑的導入，使培訓流程得以轉變爲具階段性、可觀察且可評估的能力進程，不僅提升教育的一致性，也促進課程設計、臨床表現評估與品質改善的連動 [2]。臺灣方面，急診醫學會於 2016 年率先發布全國第一版里程碑計畫，麻醉科、神經科及內科也陸續建立專科里程碑制度，逐步推進本土化 CBME 的發展 [5]。目前醫事職類則尚未發展出完整里程碑制度。

在醫事放射領域，台灣醫事放射師全國聯合會 (Taiwan Association of Medical Radiation Technologists, TAMRT) 於 2014 年建構五大核心能力，並自 2022 年起陸續建立 14 項 EPAs，做爲國內放射師專業能力架構的重要基礎。然而，除了 EPAs 之外，里程碑更能提供能力發展的層次性描述，是 CBME 系統中不可或缺的另一項關鍵工具。爲了使能力評估更爲全面，並補足核子醫學領域尚無正式里程碑架構的缺口，本研究由全聯會主導，藉由全國專家共識方法建構核子醫學里程碑，期望進一步完善台灣醫事放射職類在 CBME 架構下的教育與評估體系。

材料與方法

里程碑初稿撰寫與問卷設計

本次「放射核醫領域醫學里程碑共識」由全聯會主持，依據臺灣醫事放射師全國聯合會已建構之五大核心能力爲基礎，針對核子醫學領域建構專屬之次核心能力與學習里程碑，2024 年 1 月邀請核醫實務經驗十年以上專家小組進行草案撰寫，將五大核心能力向下延伸，撰寫核子醫學領域專屬次核心能力及對應之學習里程碑。初稿共建構 13 項次核心能力，每項次核心能力對應 5 個里程碑等級 (Level 1–5)，每一里程碑等級下有 2-5 項能力描述，所有資料彙整爲 171 項議案。所有議案以問卷方式呈現，每議案均有「維持原案」、「修改」、「刪除」或「調整等級」之選項，除「維持原案」外，其餘選項均可填寫具體修正理由。議案草案以公文方式送至全國各核醫科，收集全國初步意見。

焦點團體討論進行專家共識

專家共識於 2024 年 03 月 30 日召開，全聯會邀請全國醫事放射職類核子醫學領域醫學教育專家共 28 名出席，包括 (準) 醫學中心代表 12 位 (43%)、區域醫院代表 16 位 (57%)。由臺大醫院醫學教育專家楊志偉醫師進行里程碑介紹與共識教育訓練，爲促進專家共識形成，本研究採取「焦點團體法」(Focus Group Method) 之討論與表決程序，以確保決策客觀性與共識穩定性。針對 13 項次核心能力及其所屬里程碑共 171 項議案進行討論及表決，所有專家對於該議案無異議即直接視爲達成共識，若有專家提出意見並有專家附議即進入討論程序，經充分討論後進行表決，票數超過 80% 以上同意則該議案成立，未通過則再繼續修正與討論。

修正式德菲法進行專家共識度投票

焦點團體討論後，爲確認共識穩定性與專家一致性，進一步將獲得共識的次核心能力及里程碑，以修正式德菲法 (Modified Delphi Method, MDM) 進行共識程度投票。與會專家依據每一項次核心能力及其里程碑的「重要性」進行評分，採用五點李克特量表 ((1= 不重要，5= 非常重要)，該議案四分位差小於 0.6 且五點量表大於等於 4 則保留該案件。

結果

本研究共建構 13 項核子醫學次核心能力，分屬醫事放射師五大核心能力範疇 (表一)。在焦點團體法討論階段，討論問卷階段提出之 171 項議案，包括次核心能力與里程碑項目以及各核心能力或里程碑之新增案，經由「維持原案、修改、刪除、調整等級」等決議程序彙整後，各次核心能力之議案決議分布如表二所示。五大核心能力中，「病人照護」能力項之里程碑修改最多，其次是「醫學影像及放射科學知識」，「醫病關係及團隊溝通能力」、「提升本職技能」與「專業素養」無任何修改；自次核心項目下觀察，「同位素治療技術」爲修改最多的項目，修正 12 項里程碑議案，其次爲「核子

表一　醫事放射師五大核心能力與核子醫學次核心能力

核心能力	核子醫學次核心能力
醫學影像及放射科學知識	1. 核子醫學造影相關知識能力 2. 儀器品保與輻射安全
醫病關係及團隊溝通能力	1. 與其他專業團隊之有效溝通 2. 與病人及陪同者之妥善溝通
病人照護	1. 核子醫學造影檢查技術 2. 同位素治療技術 3. 儀器設備異常狀況處理 4. 病人安全 5. 任務交接 6. 跨領域團隊合作照護
提升本職技能	1. 提升本職技能
專業素養	1. 專業價值 2. 責任擔當

表二　核子醫學次核心能力及其里程碑之討論議案數

核子醫學次核心能力	維持原案	修改	刪除	調整等級
核子醫學造影相關知識能力	8	5	0	0
儀器品保與輻射安全	12	4	0	0
與其他專業團隊之有效溝通	10	0	0	0
與病人及陪同者之妥善溝通	11	0	0	0
核子醫學造影檢查技術	13	5	0	0
同位素治療技術	11	12	0	0
儀器設備異常狀況處理	10	1	0	0
病人安全	13	1	0	0
任務交接	10	0	0	0
跨領域團隊合作照護	10	0	0	0
提升本職技能	12	0	0	0
專業價值	11	0	0	0
責任擔當	12	0	0	0

醫學造影檢查技術」與「核子醫學造影相關知識能力」，各修正 5 項里程碑議案、「儀器品保與輻射安全」修正 4 項里程碑。

各次核心能力的最終里程碑數目介於 6 至 19 項不等，進一步以修正式德菲法 (MDM) 確認共識程度，所有平均得分皆介於 4.88–4.98 且四分位差 (IQR) 皆爲 0 (表三)。此外，各里程碑等級均依五級發展性進程進行設計，從初入職場的 Level 1，到具獨立能力的 Level 4，再到少數具專家水準者可達的 Level 5 (表四)。

討論

本研究爲臺灣首次以全國專家共識方式建構核子醫學放射師之學習里程碑，其重要性在於增添 CBME 訓練計畫中完整評量標準。過去於放射相關領域中，里程碑主要應用於醫師住院醫師訓練，例如 ACGME 所發布之 Nuclear Medicine Milestones 2.0 [2]，但針對核子醫學放射師之完整、系統化、具發展性分層之全國性里程碑架構，至今在國際間仍付之闕如。雖然美國核醫學與分子影像學會 (Society of Nuclear Medicine and Molecular Imaging – Technologist Section, SNMMI-TS) 發行的《Competency-

表三 核子醫學次核心能力最終里程碑數及共識平均值與四分位差

核子醫學次核心能力	里程碑數	平均值	四分位差
核子醫學造影相關知識能力	10	4.92	0
儀器品保與輻射安全	12	4.95	0
與其他專業團隊之有效溝通	7	4.92	0
與病人及陪同者之妥善溝通	7	4.95	0
核子醫學造影檢查技術	15	4.88	0
同位素治療技術	19	4.92	0
儀器設備異常狀況處理	8	4.93	0
病人安全	11	4.94	0
任務交接	6	4.98	0
跨領域團隊合作照護	6	4.88	0
提升本職技能	9	4.94	0
專業價值	7	4.98	0
責任擔當	8	4.95	0

表四 各項核心能力里程碑等級及其等級描述

里程碑等級	等級描述
Level 1	新進放射師的程度。
Level 2	新進放射師已經有進步但程度尚未達到中等
Level 3	新進放射師持續進步，達到該里程碑次核心能力對於新進放射師的大部分要求。
Level 4	新進放射師已經展現他達到該里程碑次核心能力對於新進放射師的訓練目標。這個等級代表他在這方面已經到達可以完訓的程度。
Level 5	新進放射師已經超越此項目對新進放射師訓練的要求，進入專家等級。只有非常少數例外的新進放射師可以達到這等級。

Based Curriculum Guide》中有列出放射師核心 / 臨床能力模組，供學程與臨床教學對齊 [6]，美國核醫技術教育審查委員會 (Joint Review Committee on Educational Programs in Nuclear Medicine Technology, JRCNMT) 於認證文件中列出 NMT competencies[7]，歐洲核醫學學會技術師委員會 EANM Technologists' Committee 亦有《Basic Benchmark》與《Advanced Benchmark》，用於訓練歐洲放射師包括放射藥學、品質控制、輻射防護、程序等能力基準與職能 [8]。但上述文件皆屬能力或課綱層級，並未提供發展進程式的行爲標準，因此本研究透過全國共同審議建構正式里程碑，可視爲臺灣核醫教育的重要創舉。

本次研究結合焦點團體法 (Focus Group Method) 與修正式德菲法 (Modified Delphi Method, MDM)，完成次核心能力與里程碑項目共 171 項次議案審議，其中 143 項次無更動 (83.6%)、28 項次修改 (16.3.%)。其中不同次核心能力的修改幅度呈現顯著差異，反映臺灣各醫院核醫科在規模、儀器配置、檢查流程與治療作業上的高度異質性，使全國共識的取得具有一定挑戰。結果顯示「同位素治療技術」修改最多 (12 項)，其次爲「核子醫學造影檢查技術」與「核子醫學造影相關知識能力」等技術導向能力，其修改率均較高；此現象與不同醫院核醫臨床任務具備流程差異與設備依賴特性一致，亦呼應國際文獻指出核醫實務較難標準化的觀察。相較之下，「溝通能力」、「團隊合作」、「專業素養」及「職責擔當」等通用能力均無需修改，顯示其行爲描述跨院所適用性高、較不受流程差異影響，因而較易形成共識。整體而言，技術性項目需更多修訂，而通用能力較爲穩定，反映核醫專業在高技術異質性與跨情境能量之間的本質差異。德菲法的量化驗證結果顯示專家對最終版本高度一致，具實施上之穩定性與信度。

透過本研究完整建構的發展式里程碑，可補足以往核醫教育中缺乏明確能力地圖的限制。在過去，核醫放射師的訓練多依賴院內師徒制與標準操作程序 (SOP)，不同院所之間的能力期待不一致，缺乏全國性標準。本

研究所建立之 Level 1–5 能力進程，使臨床教師與學習者能共享共同語言，從初學者到能獨立執行甚至具專家水準的能力變化均有具體行爲敘述。此框架提升了訓練透明度、可評估性與跨院一致性，是 CBME 精神之具體落實。加上修正式德菲法所呈現的高一致度，此里程碑架構有望成爲臺灣核醫教育的核心評量工具。

值得進一步討論的是，本研究亦提供臨床教育之重要啓示：技術類能力之高修改率反映未來課程設計與訓練標準化的優先順序。具體而言，核醫工作現場中「差異最大」的環節，如治療流程管理、緊急污染處理、特殊病例影像品質管理以及跨部門溝通，是未來需強化之要點。透過跨院案例庫建立、影像品質示例庫、治療流程模組化訓練等方法可望縮小差異，有助提升里程碑落實的可行性。

另一重要教育意義是，本研究的里程碑內容可與現行臺灣醫事放射師公會 (TAMRT) 推動之「放射師進階制度」進行銜接。進階制度將放射師職涯分爲五級，由初階、進階至專精，側重職涯能力定位；本研究里程碑則提供發展性行爲指標。兩者結合後可形成完整能力發展路徑：初階可對應 Level 1–2、進階可對應 Level 3–4、專精可對應 Level 5，使職涯制度與教育評量同步化，有助建構核醫放射師從操作能力、流程管理到跨專業協作與品質改善的垂直能力發展地圖，強化訓練體系的連貫性與可預測性。

綜合上述，本研究透過全國性、多階段、量化驗證的程序建構出具有代表性與可行性的核醫放射師里程碑，填補過往核醫教育標準與能力評估之空缺。結果顯示，不同次核心能力之修改程度反映核醫工作的技術本質與情境差異，而德菲法所得之高度一致性則支持本里程碑架構具有全國推廣的可行性。未來建議進行跨院實證研究，觀察其在不同訓練環境中的可操作性，並結合長期學習分析追蹤學員能力成長，以進一步評估里程碑的教育成效。此外，透過跨院合作建立共同課程模組與標準化能量，可望促進臺灣核醫教育更加成熟，眞正邁向與國際接軌的 CBME 教育模式。

結論

本研究運用焦點團體法建構臺灣核子醫學里程碑共識，爲 CBME 評估工具的建置奠定基礎。未來可持續追蹤里程碑的應用成效，並適時調整與精進。

致謝

本研究感謝中華民國醫事放射師公會全國聯合會 (全聯會) (TAMRT)，感謝臺大醫院醫學教育專家楊志偉醫師，也感謝本研究中的所有參與建置里程碑的核醫專家。

參考文獻

1. Dalseg, T. R., Thoma, B., Wycliffe-Jones, K., Frank, J. R., & Taber, S. (2024). Enabling implementation of competency based medical education through an outcomes-focused accreditation system. *Perspectives on Medical Education, 13*(1), 75.
2. Grayev, A., Catanzano, T. M., Sarkany, D., Winkler, N., Gaetke-Udager, K., Mian, A., Frederick, J., & Jordan, S. G. (2022). ACGME diagnostic radiology milestones 2.0: the time is now. *Academic radiology, 29*, S18-S26.
3. 蕭政廷 , 楊志偉 , & 周致丞 . (2018). 談如何在地落實 CBME: 以台灣急診醫學爲例 . *台灣醫學 , 22*(1), 55-61.
4. Frank, J. R., Snell, L. S., Cate, O. T., Holmboe, E. S., Carraccio, C., Swing, S. R., Harris, P., Glasgow, N. J., Campbell, C., & Dath, D. (2010). Competency-based medical education: theory to practice. *Medical teacher, 32*(8), 638-645.
5. 林筱茹 , 吳忠翰 , & 陳炯瑜 . (2020). 以勝任能力爲導向之醫學教育與里程碑評量 . *內科學誌 , 31*(2), 115-121.
6. SNMMI-TS Competency-Based Curriculum Guide; Society of Nuclear Medicine and Molecular Imaging Technologist Section (SNMMI-TS). *Nuclear Medicine Technology Competency-Based Curriculum Guide*. 6th ed. SNMMI; 2023. Available from: https://snmmi.org
7. JRCNMT Accreditation Standards; Joint Review Committee on Educational Programs in Nuclear Medicine Technology (JRCNMT). *Accreditation Standards for Nuclear Medicine Technologist Education.* JRCNMT; 2022. Available from: https://www.jrcnmt.org
8. EANM Basic Benchmark(2017, updated 2024); European Association of Nuclear Medicine (EANM) Technologists' Committee. *Basic Benchmark for Nuclear Medicine Technologists*. EANM; 2017. Updated online 2024. Available from: https://www.eanm.org

Establishing Milestones for the Nuclear Medicine Domain of Medical Radiation Technologists in Taiwan

Jui-Yin Kung[1,2], Hui-Ping Chen[3*], Yu-Ching Hsu[4], Chien-Jung Chen[5], Wan-Jo Chang[6], Chia-Jung Chang[7]

[1]*Department of Nuclear Medicine, Taichung Veterans General Hospital, Taichung, Taiwan*
[2]*Department of Medical Imaging and Radiological Science, Central Taiwan University of Science and Technology, Taichung, Taiwan*
[3]*Department of Nuclear Medicine, Taitung Christian Hospital, Taitung, Taiwan*
[4]*Department of Nuclear Medicine, Dalin Tzu Chi Hospital, Chiayi, Taiwan*
[5]*Department of Nuclear Medicine, National Taiwan University Hospital, Taipei, Taiwan.*
[6]*Department of Nuclear Medicine, National Taiwan University Cancer Center, Taipei, Taiwan*
[7]*Department of Nuclear Medicine, Taipei Veterans General Hospital, Taipei, Taiwan*

Abstract

To advance Competency-Based Medical Education (CBME), the Taiwan Association of Medical Radiation Technologists (TAMRT) has established five core competencies and 14 Entrustable Professional Activities (EPAs). This study aimed to develop a national consensus on Nuclear Medicine Milestones in Taiwan using the Focus Group Method as part of strengthening CBME assessment tools.

An expert panel drafted milestone descriptors for sub-competencies derived from the five core competencies, followed by a nationwide survey in March 2024. A consensus meeting was then held on March 30, 2024, with 28 nuclear medicine education experts from medical centers and regional hospitals. After literature review and consensus training, experts conducted structured discussions and voting. A total of 171 items were reviewed, resulting in 143 items retained and 28 revised. The Modified Delphi Method (MDM) was subsequently applied, yielding a consensus level of 4.93 and producing a final set of 125 Nuclear Medicine Milestones.

This study established a consensus-based milestone framework for nuclear medicine in Taiwan, providing an essential foundation for CBME-aligned assessment tools. Ongoing evaluation and refinement are recommended to ensure its continued applicability.

Keywords: Competency-Based Medical Education, Milestone, Focus Group Method, Modified Delphi Method

J Nucl Med Tech 2025;22:35-40

Received 2025/11/10
Corresponding author: Hui-Ping Chen
Address: No. 350, Kaifeng St., Taitung City, Taitung County 950405 , Taiwan (R.O.C.)
Tel: 089-960888#8172; Fax: 089-341729
E-mail: a13026@tch.org.tw

新生兒膽汁淤積 (Cholestasis) 藉由核醫檢查膽道閃爍攝影 (Cholescintigraphy) 協助診斷

蔡承延[1]　邱育琪[1]　王文祥[1]　吳宜臻[1]

[1] 義大醫院 核子醫學科

摘要

新生兒常見膽汁淤積 (Cholestasis) 的症狀，其原因有數多種，不管是肝臟本體因素或是肝臟外部原因，甚至是基因遺傳問題，皆會導致膽汁淤積在肝臟。然而，對於診斷新生兒膽汁淤積的方式也有許多管道，透過不同檢查，能更清楚診斷出新生兒膽汁淤積的原因，對於不同原因導致膽汁淤積的情況，才能更快進行相對應的治療，以達到最佳治療效果。此篇個案患者有膽汁淤積的問題，執行過多種檢查後，懷疑爲 Citrin 缺乏症導致之新生兒膽汁鬱積症 (neonatal intrahepatic cholestasis caused by citrin deficiency, 簡稱 NICCD)，後續安排至核醫科進行膽道閃爍攝影檢查，以下爲其結果及相關檢查報告。

關鍵詞：新生兒、膽汁淤積、膽道閃爍攝影

核醫技學誌 2025;22:41-45

前言

新生兒因發育尚未成熟，容易發生膽汁淤積的情形，使膽汁在肝臟內淤積無法順利排出，其原因有數多種，可能因肝臟本體原因導致，如肝炎 (新生兒肝炎及其他肝炎)、肝病 (藥物中毒性肝病及酒精性肝病)、先天性代謝疾病或代謝異常，也可能是非肝臟本體因素而導致，如膽道發育不良，或是膽道結石、腫瘤等引發膽道閉鎖。表現之臨床症狀包含黃膽、糞便尿液顏色改變及騷癢等症狀，可能伴隨肝腫大或脾腫大 [1]。然而診斷膽汁淤積的方式有很多種，可透過血液檢查發現總膽紅素 (Total-bilirubin) 或是直接型膽紅素 (Direct-bilirubin) 皆不正常上升 [2]，亦可能會進行其他基因檢查、血漿胺基酸檢查、肝功能檢查或是肝臟切片進行活組織檢查，臨床許多案例也會利用各種影像檢查進行診斷，經由腹部超音波檢查新生兒，藉由超音波影像量測膽囊大小可診斷是否爲膽道閉鎖而引起膽汁淤積，許多案例也會安排核醫檢查進行膽道閃爍攝影，用以排除膽汁淤積是否因膽道閉鎖而引起。後續會針對膽汁淤積的原因去進行各種治療，若起因爲膽道閉鎖則進行膽道手術，若是肝內代謝問題則進行藥物治療以及營養控制 [3]。

病例報告

此個案爲一男性早產兒 (34weeks)，身高爲 41.5 公分，體重爲 1720 克，APAGR score = 5/7，2025 年 03 月 22 日出生，臨床症狀有急性呼吸窘迫、腸阻塞。

2025 年 03 月 25 日執行抽血檢測，報告結果中肝發炎指數 ALT (GPT) 數值爲 23，總膽紅素數值 (T-bil) 爲 12.66mg/dL，直接型膽紅素 (D-bil) 數值爲 2.36mg/dL，T-bil 以及 D-bil 指數皆不正常升高，懷疑其有膽汁淤積

接受日期：2025 年 6 月 30 日
通訊作者：王文祥
聯絡地址：高雄市燕巢區義大路 1 號
電話：07-6150011# 2313
電子郵件：ed115123@edah.org.tw

的可能，後續則安排進行其他檢查。

2025 年 03 月 28 日執行腹部超音波檢查，肝臟無明顯腫大或異常，而膽囊 (Gallbladder) 直徑爲 1.77 公分。

2025 年 04 月 29 日抽血進行血漿胺基酸檢驗，在檢驗報告中有多種胺基酸異常，如 threonine、alanine、hydroxyproline、methionine、tyrosine、lysine、isoleucine & leucine， 若 是 有 arginine≥ 9 μmol/L、citrulline≥ 39 μmol/L、isoleucine& leucine≥ 99 μmol/L、tyrosin≥ 96 μmol/L 情況，很可能懷疑其爲 Citrin 缺乏症導致之新生兒膽汁鬱積症 (NICCD) [4]，其膽汁淤積的原因是因肝臟本體缺乏一個名爲檸檬素 (Citrin) 的運輸蛋白，肝細胞不能有效利用葡萄糖和脂肪酸產生能量，導致肝臟能量不足，此疾病爲隱性遺傳，由 SLC25A13 基因變異引起 [5]，患有此症狀的新生兒會有多重胺基酸血症、持續性黃疸、肝功能指數偏高、半乳糖血症、低蛋白血症及低血糖症現象，也可能會導致發育緩慢 [6]。

個案於 2025 年 05 月 13 日安排至核醫科進行膽道閃爍攝影，執行檢查前禁食 4 小時。靜脈注射 Tc-99m BrIDA 1mCi 後，利用伽瑪閃爍攝影機進行前位靜態照影，搭配低能量高解析度準值儀，每次收取影像以達到 200 kcts 爲止。如圖一，注射後第 5 分鐘之影像藥物已由肝完整吸收，注射後第 30 分鐘開始有腸道顯影，在注射後 1 小時收集影像完畢後即餵食牛奶，如圖二，於注射後 2 小時影像中有更多的腸道顯影，但相較於其他個案，此病患膽囊在 2 小時內未有明顯顯影，延遲至注射後 4 小時才顯影，如圖三，並加照兩側之影像以確保其顯像爲膽囊及腸道而非腎臟，確認爲膽囊顯影後，檢查即結束。

討論

此個案病患爲早產兒，出生後即具有許多臨床症狀，針對這些症狀做立即性處置後，也執行各項器官及新生兒檢查。首先，於抽血檢查時發現有許多不正常上升的數值，如 ALT、T-bil 以及 D-bil，懷疑肝臟方面有問題以及膽汁淤積可能性，後續執行許多相關檢查。

核醫的膽道閃爍攝影檢查 (Cholescintigraphy) 在協助診斷膽汁淤積爲重要角色，以此個案爲例，在餵食牛奶前後之影像皆有腸道顯像，藉此可先排除新生兒膽道閉鎖 (Biliary atresia)，以及膽道閉鎖引起膽汁淤積之可能性。接著膽囊延遲至注射藥物 4 小時後才顯影，可能原因爲新生兒肝炎 (Neonatal hepatitis)，導致無法順利排出膽汁而淤積，亦或是早產 (premature delivery)，肝臟未發育成熟，使得肝內細胞有部分東西缺乏，而其懷疑 Citrin 缺乏症導致之新生兒膽汁鬱積症 (NICCD) 則需藉由其他進一步檢查做診斷，可能進行基因檢測、肝功能測試或是膽酸檢測，若後續診斷結果確定後，則須盡快對症治療，飲食調整、藥物治療或是其他方面性治療。

參考文獻

1. 吳靜美 (2010)。肝臟的膽汁代謝功能。好心肝會刊，49 期
2. 林姿伶 (2021)。【林老師診療室】怎麼看自己的檢驗報告？膽紅素《T-Bil、D-Bil》。好心肝會刊，93 期
3. 吳嘉炀 (2013)。淺談嬰兒膽汁滯留。臺大醫院 - 健康電子報，64 期
4. Yuan-Zong Song, Kimihiko Oishi, Takeyori Saheki. Citrin Deficiency, GeneReviews, 2005
5. 尹綺琪 (2024)。香港兒童醫院 -Citrin 蛋白缺乏症 https://www31.ha.org.hk/hkch/Patients/DiseaseInfo/Citrin_Deficiency
6. 王里匀 (2011)。罕見遺傳疾病中文資料庫 -Citrin 缺乏症 https://web.tfrd.org.tw/genehelp/article.html?articleID=Citrullinemia%2520type%2520II&submenuIndex=0

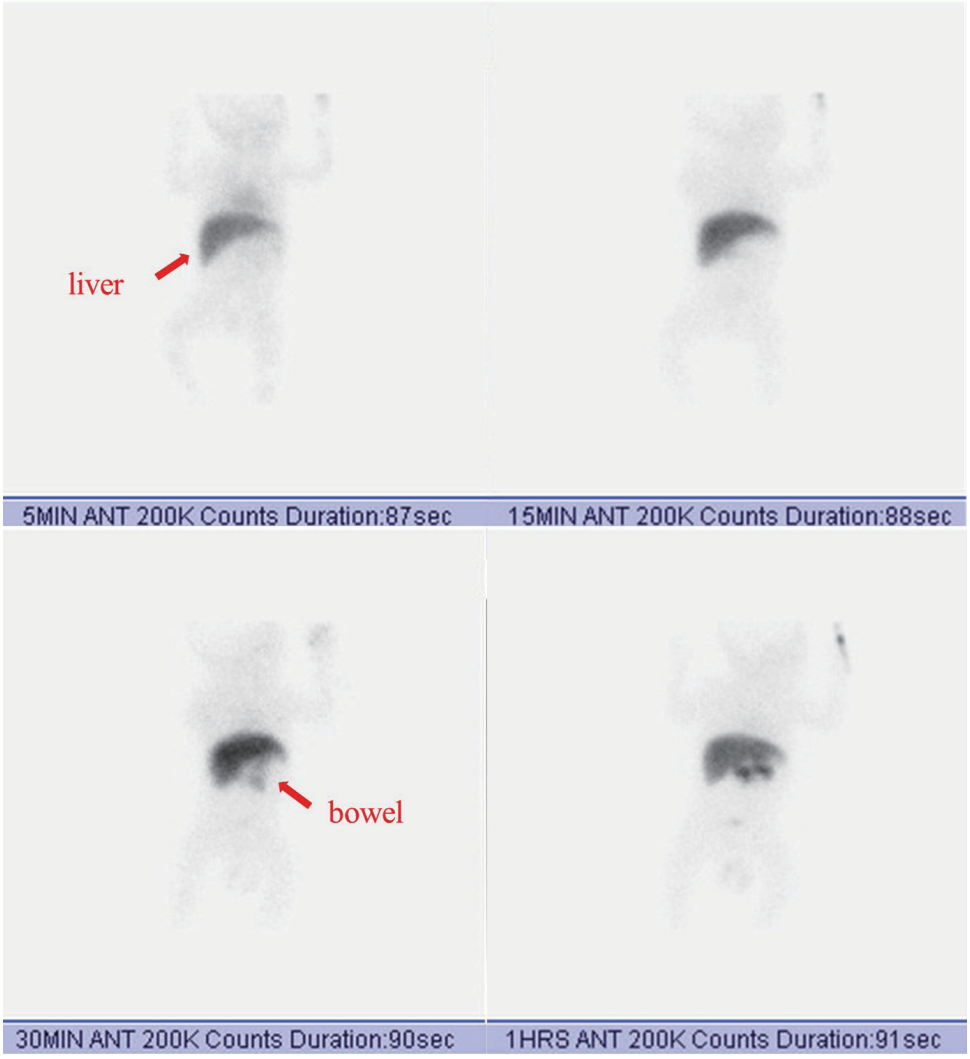

圖一　爲注射後 5 分鐘、15 分鐘、30 分鐘及 1 小時的正面靜態影像，5 分鐘時可看見肝顯影，於 30 分鐘開始腸道顯影。

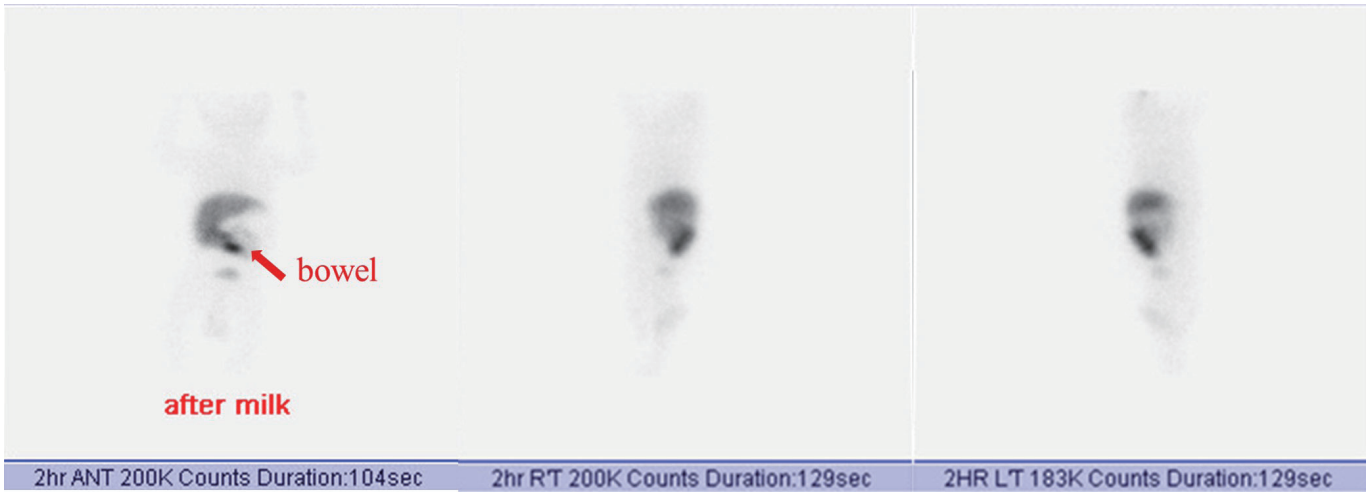

圖二 注射後 2 小時正面及側面靜態影像，餵食完牛奶後，能看見更多腸道影像。

圖三 爲注射後 4 小時正面及側面靜態影像，可看見膽囊顯影。

Neonatal Cholestasis is diagnosed by nuclear medicine examination of cholescintigraphy

Cheng-Yen Tsai[1], Yu-Ci Ciou[1], Wen-Hsiang Wang[1], Yi-Chen Wu[1]

[1]*Department of Nuclear Medicine,E-DA Hospital, Kaohsiung, Taiwan*

Abstract

Neonatal cholestasis has a wide range of potential causes, including hepatocellular dysfunction, extrahepatic obstruction, and genetic disorders, all of which can lead to bile accumulation within the liver. A variety of diagnostic approaches are available to help determine the underlying etiology. Accurate and timely diagnosis enables clinicians to implement targeted treatment strategies and improve clinical outcomes. In this case report, we present a newborn diagnosed with cholestasis. After a series of diagnostic evaluations, neonatal intrahepatic cholestasis caused by citrin deficiency (NICCD) was suspected. The patient was subsequently referred to the Department of Nuclear Medicine for a cholescintigraphy examination. The findings and relevant diagnostic reports are discussed in detail.

Keywords: neonate, cholestasis, cholescintigraphy

J Nucl Med Tech 2025;22:41-45

Received 2025/6/30
Corresponding author: Wen-Hsiang Wang
Address: No.1, Yida Road, Jiaosu Village, Yanchao District, Kaohsiung City 82445, Taiwan, R.O.C.
Tel: 07-6150011# 2313
E-mail: ed115123@edah.org.tw

PET Respiratory Motion Management in Lung and Liver Metastasis

Ruo-Ning Sun[1], Yen-Kung Chen[2,3]

[1]*Siemens Healthcare Limited, Taiwan*
[2]*Department of Nuclear Medicine and PET Center, Shin Kong Wu Ho-Su Memorial Hospital, Taipei, Taiwan*
[3]*School of Medicine, Fu Jen Catholic University, New Taipei City, Taiwan*

Abstract

Introduction: Respiration gating is used in PET scan to prevent image quality degradation due to respiratory effects.

Case presentation: This is a 69-year-old man who had an underlying disease right lower lobe lung adenocarcinoma, cT3N3M1c, stage IVB, contralateral lung/liver/pancreas metastasis, post concurrent chemoradiotherapy; post thoracoscopic right lower lung lobectomy; left upper lobe metastatic lung cancer, post video-assisted thoracic surgical wedge resection; post thoracoscopic wedge resection for right upper lobe lung nodule; pancreatic metastasis, post ERCP with FNB, EST, and biliary plastic stenting. The recent FDG PET/CT scan revealed the following: Progressive metastases in the bilateral lungs, mediastinal and abdominal lymphadenopathy, left adrenal gland, bilateral hepatic lobes, and muscle (right scapula, right lower lateral chest wall, right para T10/11 vertebra). Progressive pancreatic malignancy in both the head and tail, which could be primary or metastatic; the tail portion is occupied by left adrenal metastasis. Some focus with FDG uptake in the lung and liver presents long shape and blurred appearance due to respiration motion. After using an image with data-driven respiratory gating and motion correction, focus with FDG uptake in the lung and liver become ring shape and more intense FDG uptake..

Conclusion: Respiratory motion compensation techniques allow superior FDG PET image quality without causing prolonged scan time.

Keywords: respiratory motion management, lung adenocarcinoma, lung metastasis, liver metastasis, FDG PET/CT

J Nucl Med Tech 2025;22:47-53

Received 2025/8/4
Corresponding author: Yen-Kung Chen
MD, PhD, Department of Nuclear Medicine and PET Center, Shin Kong Wu Ho-Su Memorial Hospital
Address: No. 95, Wen Chang Rd., Shih Lin District, Taipei, Taiwan
Phone: 886-2-2833-2211 EXT 2280 Fax: 886-2-2838-9489
E-mail: M004149@ms.skh.org.tw

INTRODUCTION

Respiratory motion can cause blurring in positron emission tomography (PET) imaging modality. Image acquisition for PET requires several minutes, so lesion blurring due to respiratory motion is common. This can lead to an over-estimation of lesion volume, as well as under-estimation of radionuclide uptake by the lesion (as standardized uptake value (SUV)). Respiration motion induced image degradation may be present from the apex of the lung to the lower abdomen, and particularly near the diaphragm which has been shown to move 8–25 mm during breathing [Hamill, 2008]. Respiratory motion of organs and lesions are unavoidable during the PET data acquisition resulting in degraded PET image quality due to blurring that effectively lowers the spatial resolution [Büther, 2020]. Small peri-diaphragmatic lesions may therefore be

undetectable in some patients and the measured SUV values may be underestimated. So, corrected respiration motion PET imaging could improve lesion detection, characterization, and quantification (Dias, 2022).

Case Report

A 69-year-old male was diagnosed with RLL lung adenocarcinoma on April 13, 2020. Initial staging revealed an EGFR mutation (Exon 21 Leu858Arg). He received neoadjuvant concurrent chemoradiotherapy (CCRT) with Navelbine/Cisplatin, followed by thoracoscopic right lower lobe lobectomy and mediastinal lymph node dissection on July 14, 2020. Post-surgery, the patient underwent adjuvant chemotherapy with oral NVB + CDDP.

On January 27, 2021, a follow-up FDG PET/CT scan revealed bone (L1 vertebra), bilateral lung, right pleura, and adrenal metastases. Afatinib + Xgeva were administered. A brain MRI performed on February 4, 2021, disclosed a dural tumor with peritumoral edema and bony invasion, consistent with metastasis. The patient was referred for palliative radiotherapy.

Subsequent FDG PET/CT scans on June 21, 2022, showed nodular lesions in the right pleura, suspected to be pleural metastasis. A CT scan on September 8, 2022, identified newly enlarged nodules in the LUL (1.4 cm and 0.8 cm) and LLL (0.6 cm), along with a pancreatic head mass (2.1 cm). On September 27, 2022, an EUS biopsy confirmed small-cell neuroendocrine carcinoma in the pancreas. The patient was diagnosed with adenocarcinoma, EGFR-mutant, with small-cell transformation and pancreatic metastasis.

He underwent 6 courses of chemotherapy with VP16 + CDDP, achieving a good response in the pancreatic tumor. However, a CT on March 24, 2023, revealed progressive nodules in the LUL, LLL, RUL, and RML. He subsequently underwent a wedge resection of LUL nodules, and pathology confirmed adenocarcinoma with an EGFR Exon 21 mutation. Erlotinib was initiated, but the patient developed shortness of breath and was diagnosed with Erlotinib-induced pneumonitis. After a temporary suspension of Erlotinib, the drug was reintroduced, but disease progression was observed in the lungs, adrenal gland, and pancreas.

Chemotherapy was switched to Taxotere + Paraplatin. A CT scan on December 14, 2023, showed multiple metastatic lesions in the lungs, adrenal glands, and bones, with most lesions increasing in size, consistent with progressive disease. The pancreatic head tumor, however, had decreased in size.

The patient was admitted for re-biopsy in January 2024 and underwent a thoracoscopic wedge resection of the right upper lobe. Pathology confirmed adenocarcinoma with the same EGFR mutation. Chemotherapy was switched to Iressa. The patient recently developed tea-colored urine, vomiting, and significant weight loss, with liver function tests revealing elevated AST/ALT, bilirubin, and alkaline phosphatase. An abdominal ultrasound revealed an enlarged pancreatic tail tumor (7 cm), dilated MPD and CBD, and biliary obstruction. ERCP with biliary stenting was performed, and pathology confirmed small-cell carcinoma.

The patient received four cycles of PARAPLATIN + Fytosid. A recent FDG PET/CT scan showed progressive metastases in the lungs, liver, and adrenal gland, along with an increased pancreatic mass. The patient reported dyspnea, poor appetite, and an 11 kg weight loss over recent months. He was admitted for cycle 5 chemotherapy with reduced VP16 + Carboplatin, along with Filgrastim.

Discussion

This patient had an underlying disease right lower lung adenocarcinoma, cT3N3M1c, stage IVB, contralateral lung/liver/pancreas metastasis, post concurrent chemoradiotherapy; post thoracoscopic right lower lung lobectomy; left upper lobe metastatic lung cancer, post video-assisted thoracic surgical wedge resection; post thoracoscopic wedge resection for right upper lobe lung nodule. He referred to this FDG PET/CT scan for restaging and therapeutic response. He felt dyspnea on exertion, especial go up to second floor. Although pulmonary function test reporter normal spirometry and lung volumes.

During the fusion of PET and CT, artifacts may occur due to respiratory motion, metallic implants, CT contrast

media, and truncation. Among them, respiratory motion artifacts are one of the most common and important artifacts in PET/CT. Respiratory motion is greater in the lower lobe than in the upper lobe, moves mainly in the superior-inferior direction. [Lupi, 2009]. Nii et al. showed a trend toward a greater correction effect on respiratory motion in the lower lobe than in the upper lobe [Nii, 2023]. The gating method has been attempted to reduce artifacts caused by respiratory motion on PET/CT, using an external sensor, such as a pressure belt or a video camera. However, there is a limitation to the use of respiratory gating methods because an additional external device is required for gating, or some PET/CT devices do not support such methods.

In the prone position, the spontaneous effort of breathing decreases [Yoshida, 2022]. Moreover, since the movement of the diaphragm in the prone position is reduced [Nam, 2010], prone position PET/CT might also be helpful in evaluating hepatic lesions located close to the diaphragm. However, pPET/CT has multiple disadvantages; for example, it requires additional radiation exposure and extends the image acquisition time [Lee, 2023].

OncoFreeze (Siemens Healthineers) is a type of respiration gating software that combines continuous bed motion and device- and amplitude-based PET gating with elastic motion compensation [Pösse, 2020]. OncoFreeze provides a new respiration gating function based on HD-Chest (Siemens) technology that does not require an increase in imaging time. OncoFreeze uses a mass-preserving optical flow to generalize respiratory motion and reconstructs the image using all breath-count data from the HD-Chest image as a reference. OncoFreeze AI (Siemens Healthineers), a data-driven deviceless respiration gating system, was later created [Walker, 2019; Büther, 2020]. OncoFreeze AI extracts respiratory waveforms for each patient from continuous PET data using FlowMotion technology (Siemens Healthineers) and reconstructs respiration-gated images based on those respiratory waveforms. OncoFreeze AI estimates the respiratory waveform based on the features of DDG and FlowMotion. Data-driven respiration gating was performed on 38 lung lesions in a CBM ^{18}F-FDG PET study and significantly increased SUV and decreased MTV compared with no gating. Although data-driven deviceless respiration-gated reconstruction assumes the presence of respiratory motion, the phantom test results did not impair quantification in regions where respiratory motion was absent [Nii, 2023].

Conclusion

Respiratory motion compensation using data-driven deviceless respiration gating system is readily integrated into clinical routine and produce images with more accurate and significantly greater SUV values and smaller metabolic volumes.

References

1. Hamill J, Bosmans G, Dekker A. Respiratory-gated CT as a tool for the simulation of breathing artifacts in PET and PET/CT. Med Phys. 2008;35:576–85. https://doi.org/10.1118/1.2829875.
2. Büther F, Jones J, Seifert R, Stegger L, Schleyer P, Schäfers M. Clinical evaluation of a data-driven respiratory gating algorithm for whole-body PET with continuous bed motion. J Nucl Med. 2020;61:1520–7. https://doi.org/10.2967/jnumed.119.235770.
3. Dias, A.H., Schleyer, P., Vendelbo, M.H. et al. Clinical feasibility and impact of data-driven respiratory motion compensation studied in 200 whole-body ^{18}F-FDG PET/CT scans. EJNMMI Res 12, 16 (2022). https://doi.org/10.1186/s13550-022-00887-x.
4. Pösse S, Büther F, Mannweiler D, et al. Comparison of two elastic motion correction approaches for whole-body PET/CT: motion deblurring vs gate-to-gate motion correction. EJNMMI Phys. 2020;7:19.
5. Nii T, Hosokawa S, Kotani T, Domoto H, Nakamura Y, Tanada Y, Kondo R, Takahashi Y. Evaluation of Data-Driven Respiration Gating in Continuous Bed Motion in Lung Lesions. J Nucl Med Technol. 2023 Mar;51(1):32-37. doi: 10.2967/jnmt.122.264909. Epub 2023 Feb 7. Erratum in: J Nucl Med Technol. 2023 Jun;51(2):159. PMID: 36750380.

6. Lupi A, Zaroccolo M, Salgarello M, Malfatti V, Zanco P. The effect of ^{18}F-FDG PET/CT respiratory gating on detected metabolic activity in lung lesions. Ann Nucl Med. 2009;23:191–196.
7. Walker MD, Morgan AJ, Bradley KM, McGowan DR. Evaluation of data-driven respiratory gating waveforms for clinical PET imaging. EJNMMI Res. 2019;9:1.
8. Büther F, Jones J, Seifert R, Stegger L, Schleyer P, Sch∈afers M. Clinical evaluation of a data-driven respiratory gating algorithm for whole-body PET with continuous bed motion. J Nucl Med. 2020;61:1520–1527
9. Yoshida, T.; Engelberts, D.; Chen, H.; Li, X.; Katira, B.H.; Otulakowski, G.; Fujino, Y. Prone position minimizes the exacerbation of effort-dependent lung injury: Exploring the mechanism in pigs and evaluating injury in rabbits. Anesthesiology 2022, 136, 779–791.
10. Nam, Y.; Yoon, A.M.; Kim, Y.H.; Yoon, S.H. The effect on respiratory mechanics when using a Jackson surgical table in the prone position during spinal surgery. Korean J. Anesthesiol. 2010, 59, 323–328.
11. Lee, C.W.; Son, H.J.; Woo, J.Y.; Lee, S.H. Is Prone Position [18F]FDG PET/CT Useful in Reducing Respiratory Motion Artifacts in Evaluating Hepatic Lesions?. Diagnostics 2023, 13, 2539. https://doi.org/10.3390/ diagnostics13152539

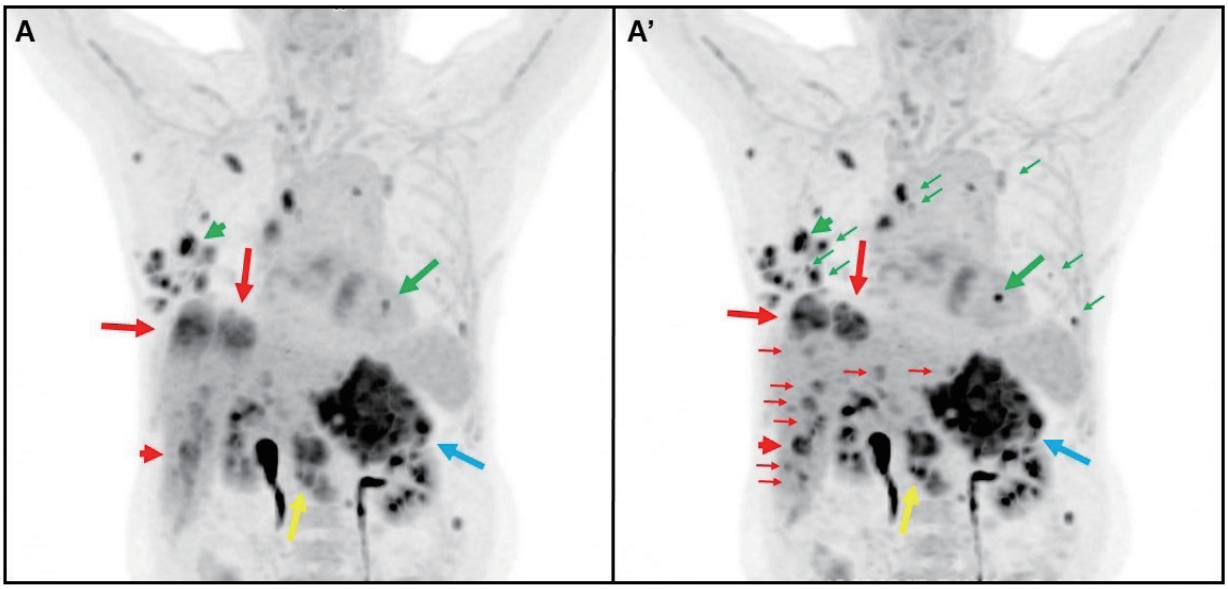

Figure 1. A 69-year-old man had an underlying disease right lower lung adenocarcinoma, cT3N3M1c, stage IVB, contralateral lung/liver/pancreas metastasis, s/p CCRT; s/p thoracoscopic right lower lung lobectomy; left upper lobe metastatic lung cancer, post video-assisted thoracic surgical wedge resection; s/p thoracoscopic wedge resection for right upper lobe lung nodule. He was referred for FDG-PET/CT to evaluate the extent of the disease. Respiration-gated images (OncoFreeze AI with data-driven respiration gating; A', MIP images of PET) and ungated images (static; A, MIP images of PET) were reconstructed. The red (long and short thick, thin) arrow indicates liver metastasis with increased to intense FDG uptake. The green (long and short thick, thin) arrow indicates lung metastasis with increased to intense FDG uptake. Pancreatic metastasis (4.1 cm, yellow arrow) and left adrenal metastasis (9.9 cm, blue arrow) was noted.

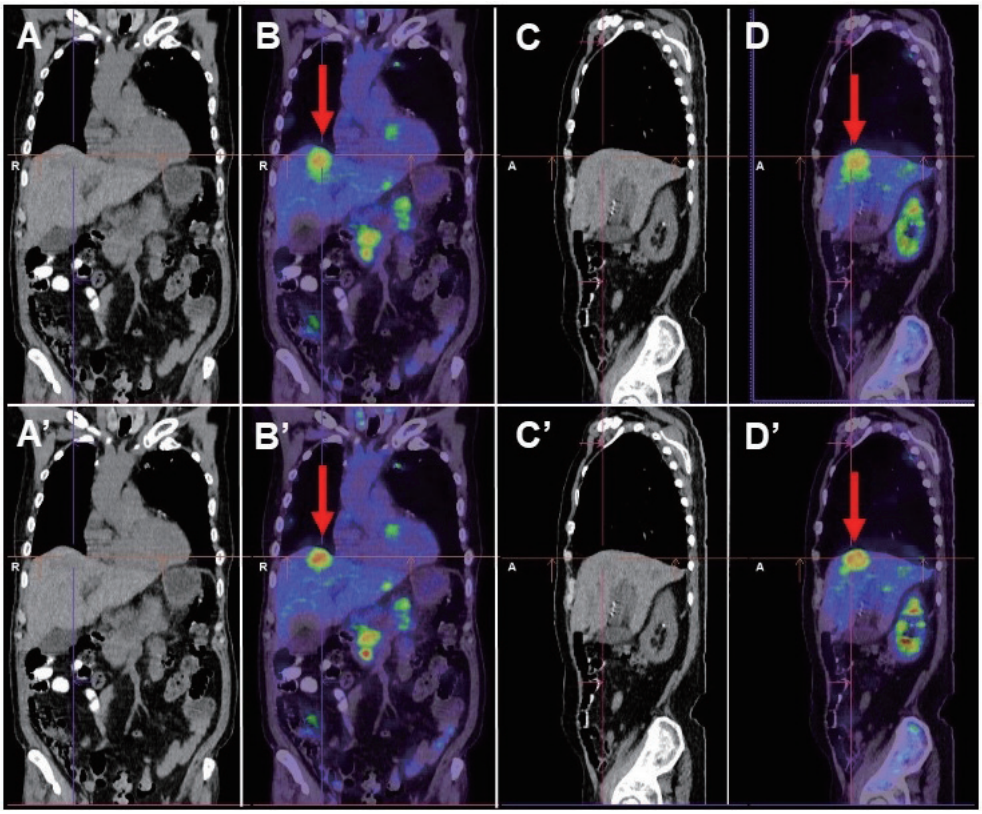

Figure 2. The red long thick arrow indicates a focal area with heterogeneous increased FDG uptake in the liver S8. (A, A': coronal CT; B, B': coronal PET/CT fusion; C, C': sagittal CT; D, D': sagittal PET/CT fusion). Respiration-gated images (OncoFreeze AI with data-driven respiration gating; A', B', C' and D') and ungated images (static; A, B, C, D) were reconstructed. The liver S8 lesion measured maxSUV 7.6, meanSUV 5.1 and metabolic tumor volume 19.1 cm^3 in ungated images (static; A, B, C, D). The liver S8 lesion measured maxSUV 8.7, meanSUV 6.1 and metabolic tumor volume 13 cm^3 in respiration-gated images (OncoFreeze AI with data-driven respiration gating; A', B', C' and D'). The liver S8 lesion measured in CT image (2.6x2.3 cm), ungated images (2.6x2.9 cm) and respiration-gated images (2.6x2.5 cm).

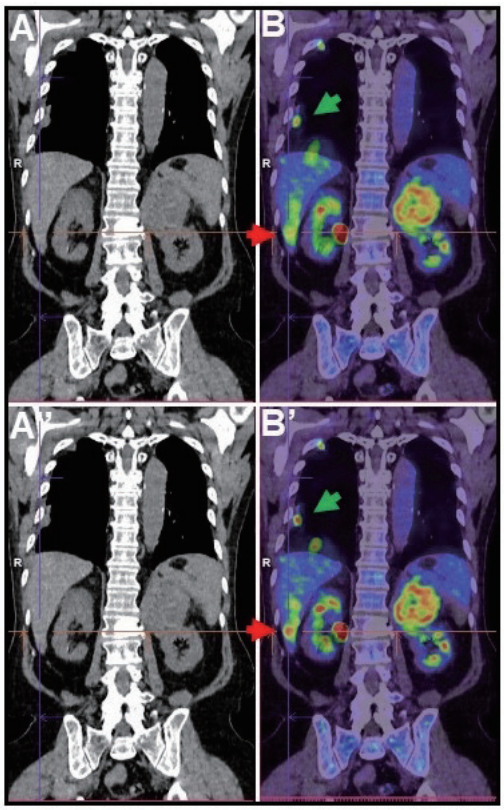

Figure 3. The red and green short thick arrow indicates a focal area with increased FDG uptake in the liver S6 and right lower lung attached to pleura, respectively. (A, A': coronal CT; B, B': coronal PET/CT fusion). Respiration-gated images (OncoFreeze AI with data-driven respiration gating; A' and B') and ungated images (static; A and B) were reconstructed. The liver S6 lesion measured maxSUV 8.0, meanSUV 5.7 and metabolic tumor volume 2.65 cm3 in ungated images (static; A, B). The liver S6 lesion measured maxSUV 10.7, meanSUV 7.3 and metabolic tumor volume 2.46 cm3 in respiration-gated images (OncoFreeze AI with data-driven respiration gating; A', B'). The right lower lung lesion measured maxSUV 8.0, meanSUV 4.5 and metabolic tumor volume 1.56 cm3 in ungated images (static; A, B). The right lower lung lesion measured maxSUV 12.1, meanSUV 8.3 and metabolic tumor volume 0.8 cm3 in respiration-gated images (OncoFreeze AI with data-driven respiration gating; A', B').

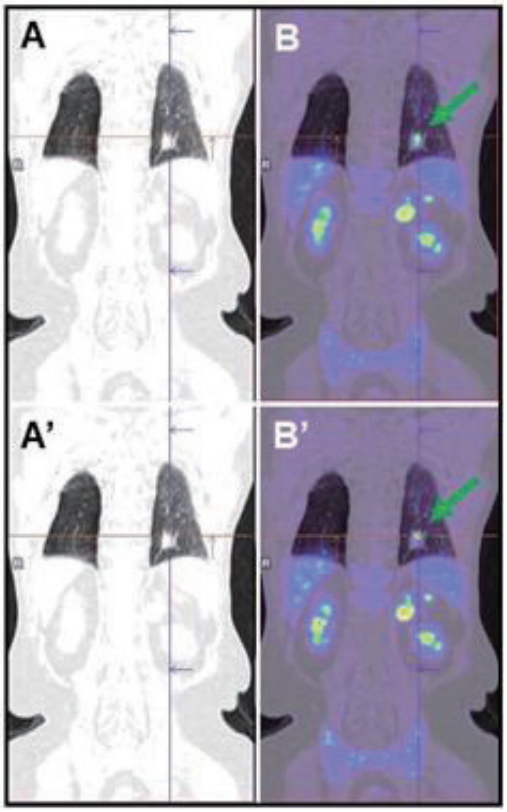

Figure 4. The green long thick arrow indicates a focal area with increased FDG uptake in the left lower lung. (A, A': coronal CT; B, B': coronal PET/CT fusion). Respiration-gated images (OncoFreeze AI with data-driven respiration gating; A' and B') and ungated images (static; A and B) were reconstructed. The left lower lung lesion measured maxSUV 5.9, meanSUV 3.2 and metabolic tumor volume 1.3 cm3 in ungated images (static; A, B). The left lower lung lesion measured maxSUV 10.5, meanSUV 7.1 and metabolic tumor volume 0.3 cm3 in respiration-gated images (OncoFreeze AI with data-driven respiration gating; A', B').

肺和肝轉移正子斷層造影的呼吸運動管理

孫若寧[1]　陳遠光[2,3]

[1] 西門子醫療
[2] 新光吳火獅紀念醫院核子醫學科暨正子斷層造影中心
[3] 台灣新北市輔仁大學

中文摘要

引言

呼吸門控用於 PET 掃描，以防止呼吸影響導致影像品質下降。

病例介紹

69 歲男性，潛在疾病爲右下葉肺腺癌，cT3N3M1c，IVB 期，對側肺 / 肝 / 胰臟轉移，同步放化療後；胸腔鏡右下肺葉切除術後；左上葉轉移性肺癌，影片輔助胸腔外科楔形切除術後；胸腔鏡下右上葉肺結節楔形切除術；胰臟轉移、ERCP 後 FNB、EST 和膽道塑膠支架置入術。最近的 FDG PET/CT 掃描顯示：雙側肺部進行性轉移、縱隔和腹部淋巴結腫大、左腎上腺、雙側肝葉和肌肉 (右肩胛骨、右下外側胸壁、右 T10/11 椎旁)。頭部和尾部進行性胰臟惡性腫瘤，可能是原發性或轉移性；尾部被左腎上腺轉移佔據。由於呼吸運動，肺部和肝臟中一些 FDG 攝取的病灶呈現出長形和模糊的外觀。使用具有數據驅動的呼吸門控和運動校正的影像後，肺部和肝臟中 FDG 攝取的焦點變成環形並且 FDG 攝取更強烈。

結論

呼吸運動補償技術可實現卓越的 FDG PET 影像質量，而不會導致掃描時間延長。

關鍵字：呼吸運動管理、肺腺癌、肺轉移、肝轉移、氟化去氧葡萄糖正子電腦斷層造影

核醫技學誌 2025;22:47-53

接受日期：2025 年 8 月 4 日
通訊作者：陳遠光
聯絡地址：台北市士林區文昌路 95 號 新光吳火獅紀念醫院核子醫學科
聯絡電話：02-28332211 ext 2280；傳眞：02-28389489
電子郵件：M004149@ms.skh.org.tw

心肌灌注掃描檢查意外發現肺腫瘤活性吸收

朱秀蘭[1]　游慧貞[2]

[1] 高雄醫學大學附設中和紀念醫院 核子醫學部
[2] 高雄醫學大學附設中和紀念醫院 影像醫學部

摘要

本次病例報告討論一位男性心臟病患者，在執行心肌灌注掃描檢查時，發現在右上肺葉部有 TL-201 活性異常吸收，查核患者病史，發現其過往曾患直腸癌且已治療且透過 CT 檢查亦曾發現右上肺葉部有 2 公分的腫塊。TL-201 不僅適用於心肌灌注評估，更可透過聚積於代謝活躍腫瘤細胞進行癌症造影。

關鍵詞：TL-201，心肌灌注掃描，鉈 -201 癌症追蹤掃描

核醫技學誌 2025;22:55-58

接受日期：2025 年 11 月 26 日
通訊作者：游慧貞
聯絡地址：高雄市三民區十全一路 100 號
電話：07-3121101 轉 7721
電子郵件：I760192@yahoo.com.tw

前言

據衛生福利部統計，心臟疾病發生率居高不下，其中最多數便是冠狀動脈疾病 (coronary artery disease, CAD)。核醫科的心肌灌注掃描便可用於評估心臟肌肉的血液供應狀況及冠狀動脈疾病之診斷，進一步評估疾病的影響範圍與嚴重程度 [1-2]。檢查過程包括壓力相及休息相兩個階段，患者需先注射放射性同位素 (如 TL-201 或 ^{99m}TC-MIBI)，然後進行單光子電腦斷層掃描 (SPECT)。因 TL-201 類似鉀離子，會經由 Na^+/K+ATPase system 主動運輸之機轉進入心肌細胞內，TL-201 被心肌細胞攝取比例與血流量及細胞存活程度成正比，便可反應冠狀動脈血流供應量，進而評估心肌缺氧狀況 [3-4]。

TL-201 不僅可以用於心肌灌注掃描檢查，也可以做爲癌症追蹤檢查放射藥劑，因 TL-201 也可經由 Na^+/K^+ATPase system 聚集在代謝旺盛的腫瘤細胞，加上腫瘤細胞長速度快，具有豐富的血流，促使腫瘤細胞部位的 Tl-201 含量增加，可以做腫瘤造影，臨床上常使用在腫瘤分期、決定 biopsy 的位置、評估癌症於治療前後之情形等。其適應症爲甲狀腺癌、腦瘤、骨骼軟組織腫瘤、肺癌、頭頸部癌等癌症 [5-9]。

病例報告

本次案例爲 84 歲男性心臟病患者，於 2023 年 11 月進行心肌灌注掃描檢查時，發現在右上肺葉部有 TL-201 活性異常吸收 (圖一、二)，經檢視患者病史發現其過往曾患直腸癌且已治療，此後有呼吸窘迫之症狀。查核患者於 2023 年 2 月透過 CT 檢查亦曾發現右上肺葉部有 2 公分的腫塊 (圖三)，同年 5 月再做 CT 檢查追蹤時，發現腫塊成長爲 2.34 公分 (圖四)。因患者腎臟功能差，

兩次 CT 檢查皆未打顯影劑，無病理檢查報告，故無法確定其爲良性或惡性腫瘤。截至 2025 年 1 月並未有進一步檢查或處理腫瘤紀錄。

討論

TL-201 憑藉其 Na^+/K^+ATPase system 親和性，不僅適用於心肌灌注評估，更可透過聚積於代謝活躍腫瘤細胞進行癌症造影，在甲狀腺癌、腦瘤等多種惡性腫瘤的分期、定位及療效評估中具有重要臨床價值。

參考文獻

1. Gerson, M. C., “Cardiac Nuclear Medicine,” 2nd., Mc Graw-Hill Inc, New York, pp. 273-418, 1991.
2. Pepine, C. J., Nichols, W. W., “The pathophysiology of chronic ischemic heart disease,” Clin Cardiol. Vol. 30, No.2, 2007, pp: I4-I9.
3. Clark, A.N., Beller, G.A., “The present role of nuclear cardiology in clinical practice,” Q J Nucl Med Mol Imaging. Vol. 49, No. 1, 2005, pp: 43-58.
4. Koshino, K., Fukushima, K., Fukumoto, M., et al., “Quantification of myocardial blood flow using (201) Tl SPECT and population-based input function,” Ann Nucl Med. Vol. 28, No. 9, 2014, pp: 917-925.
5. McKillop JH. Thallium 201 scintigraphy. West J Med 1980;133:26-43.
6. Waxman AD. Thallium in nuclear oncology Nuclear Medicine Annual, Raven, New York (1991), pp:193-209.
7. Chin BB, Zukerberg BW, Buchpiguel C, Alavi A. Thallium-201 uptake in lung cancer. J Nucl Med 1995;36:1514-1519.
8. Van der Wall H, Murray IP, Huckstep RL, Philips RL. The role of 201Tl scintigraphy in excluding malignancy in bone. Clin Nucl Med, 1993; 18(7):551-557.
9. Kostakoglu L, Panicek DM, Divgi CR, et al. Correlation of the findings of thallium-201 chloride scans with those of other imaging modalities and histology following therapy in patients with bone and soft tissue sarcomas. Eur J Nucl Med 1995;22:1232-1237.

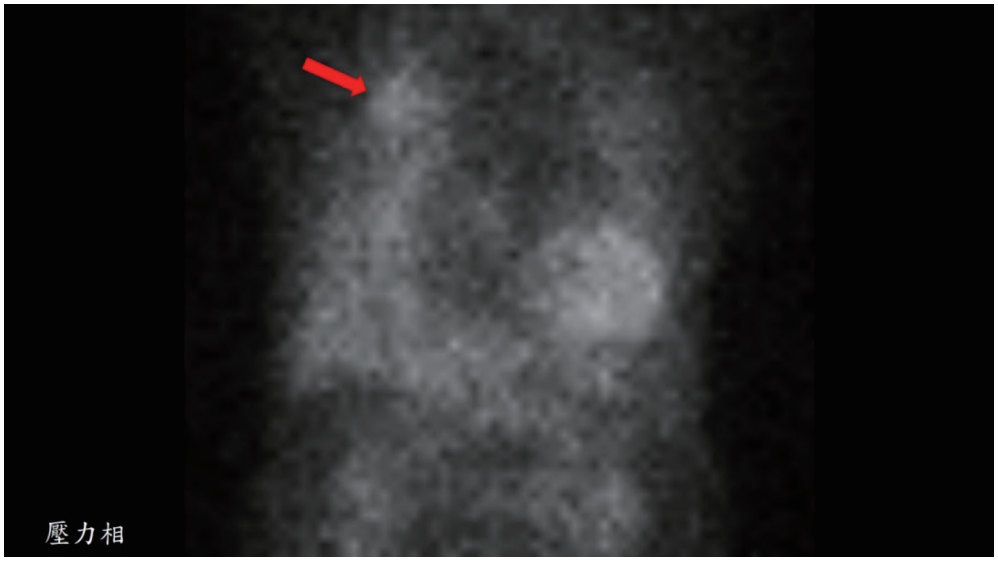

圖一　心肌灌注掃描壓力相中，發現在右上肺葉部有 TL-201 活性異常吸收。

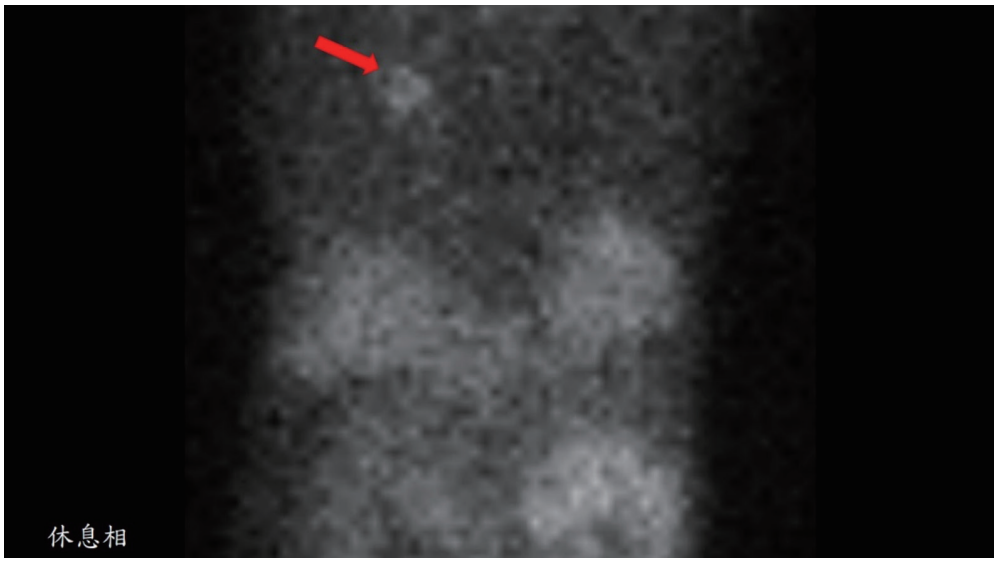

圖二　心肌灌注掃描休息相中，發現在右上肺葉部有 TL-201 活性異常吸收。

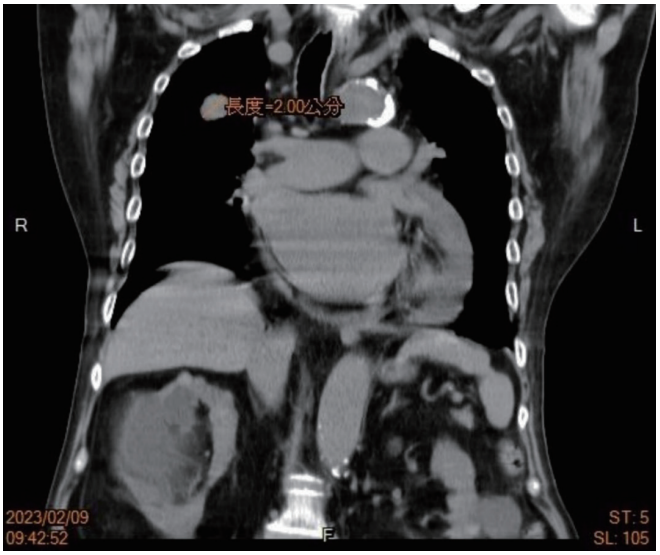

圖三　患者於 2023 年 2 月透過 CT 檢查，發現右上肺葉部有 2 公分的腫塊。

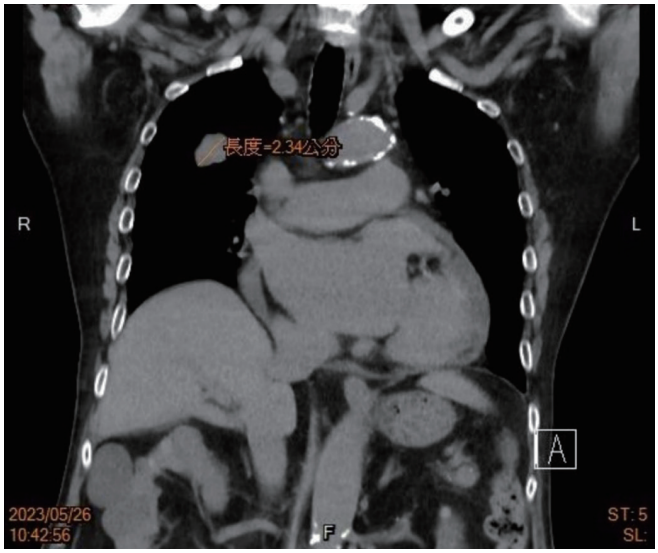

圖四　查核患者於 2023 年 5 月透過 CT 檢查追蹤，發現腫塊成長爲 2.34 公分。

Incidental Thallium-201 Uptake in a Lung Tumor on Myocardial Perfusion Imaging

Hsiu-Lan Chu[1], Hui-Chen Yu[2]

[1]*Department of Nuclear Medicine, Kaohsiung Medical University Hospital, Kaohsiung Medical University, Kaohsiung, Taiwan*
[2]*Department of Medical Imaging, Kaohsiung Medical University Hospital, Kaohsiung Medical University, Kaohsiung, Taiwan*

Abstract
This case report presents a male patient with underlying cardiac disease who underwent Thallium-201 (Tl-201) myocardial perfusion imaging (MPI). The scan revealed incidental abnormal Tl-201 uptake in the right upper lobe (RUL) of the lung. A review of the patient's medical history disclosed a history of treated rectal cancer, and a prior computed tomography (CT) scan had identified a 2-cm mass in the right upper lobe. Tl-201 is not only useful for myocardial perfusion assessment but also demonstrates utility in tumor imaging due to its accumulation in metabolically active tumor cells.

Keywords: TL-201, Myocardial Perfusion Scan, Tl-201 Cancer Work Up Scan

J Nucl Med Tech 2025;22:55-58

Received 2025/11/26
Corresponding author: Hui-Chen Yu
Address: No.100, Tzyou 1st Road Kaohsiung 807, Taiwan
Tel: 07-3121101# 7721
E-mail: I760192@yahoo.com.tw